Composite Structures 86 (2008) 328–343

Contents lists available at ScienceDirect

Composite Structures

journal homepage: www.elsevier.com/locate/compstruct

Static deformations and vibration analysis of composite and sandwich plates using a layerwise theory and RBF-PS discretizations with optimal shape parameter

A.J.M. Ferreira [a,*], G.E. Fasshauer [b], R.C. Batra [c], J.D. Rodrigues [a]

[a] Departamento de Engenharia Mecânica e Gestão Industrial, Faculdade de Engenharia da Universidade do Porto, Rua Dr. Roberto Frias, 4200-465 Porto, Portugal
[b] Department of Applied Mathematics, Illinois Institute of Technology, Chicago, IL 60616, USA
[c] Department of Engineering Science and Mechanics, MC0219, Virginia Polytechnic Institute and State University, Blacksburg, VA 24061, USA

ARTICLE INFO

Article history:
Available online 5 August 2008

Keywords:
Sandwich plates
Mode shapes
Radial basis functions
Frequencies

ABSTRACT

A study of static deformations and free vibration of shear flexible isotropic and laminated composite plates is presented. A layerwise theory for laminated or sandwich plates is used. The analysis is based on a new numerical scheme, where collocation by radial basis functions is viewed as a pseudospectral method to produce highly accurate results. A cross-validation technique is used to optimize the shape parameter for the basis functions. Numerical results for symmetric laminated composite and sandwich plates are presented and discussed.

1. Introduction

Due to the high ratio of tensile modulus to transverse shear modulus in composite materials, the use of shear deformation theories is of crucial importance in static and dynamic analysis of composite and sandwich laminates.

The classical laminate plate theory and the first-order shear deformation theory [1–3] are the most typical and used deformation theories for the analysis of composite laminates. Higher-order theories can also be used, with advantages regarding the warping of the normal to the middle surface. Such theories also have the advantage of disregarding shear correction factors and may yield more accurate transverse shear stresses [4–10]. Classical, first-order or higher-order theories also consider laminate-wise rotations. However, in some laminates, particularly in sandwich applications, the difference between material properties suggests the use of layerwise theories, that consider independent degrees of freedom for each layer. The layerwise theory of Reddy [11] is perhaps the most popular layerwise theory for composite and sandwich plate analysis. In this work, we adopt a layerwise theory based on an expansion of Mindlin's first-order shear deformation theory in each layer. The displacement continuity at layer's interface is guaranteed and produces very accurate transverse shear stress, in each layer middle surface. Other layerwise or zig-zag theories have been presented by Mau [6], Chou and Corleone [12], Di Sciuva [13], Murakami [14], Ren [15]. A recent and comprehensive review of such theories in the analysis of multilayered plates and shells has been presented by Carrera [16].

Most of the spacial discretization techniques so far have been based on finite differences and finite elements. In this study, a layerwise shear deformation theory is implemented in a new numerical scheme where collocation by radial basis functions is viewed as a pseudospectral method to produce highly accurate results. In this paper, we use a cross-validation technique to optimize the shape parameter for the basis functions.

The radial basis function method was first used by Hardy [17,18] for the interpolation of geographical scattered data and later used by Kansa [19,20] for the solution of partial differential equations (PDEs). Many other radial basis functions can be used as reviewed in the recent book of Liu [21] and in the recent works [22–27]. The method has also been applied to other engineering problems such as in [28–31]. The use of RBFs for 2D solids has been proposed by Liu et al. [32–34] and by Ferreira [35–37] for composite laminated plates and beams using the first-order and the third-order shear deformation theory. The use of layerwise theories and radial basis functions has also been proposed recently by Ferreira et al. for the static deformations of composite plates in bending [38,39]. In this paper, we combine for the first time a layerwise theory for plates, a radial basis method with pseudospectral framework and an optimization technique of the shape parameter.

2. RBF–PS methods

Pseudospectral (PS) methods (see the books [40] or [41] for an introduction to the subject) are known as highly accurate solvers for partial differential equations (PDEs). Generally speaking, one represents the spatial part of the approximate solution $\hat{u}$ of a given PDE by a linear combination of certain smooth basis functions $\phi_j, j = 1, \ldots, N$, i.e.,

* Corresponding author.
E-mail addresses: ferreira@fe.up.pt (A.J.M. Ferreira), fasshauer@iit.edu (G.E. Fasshauer), rbatra@vt.edu (R.C. Batra), jdr@fe.up.pt (J.D. Rodrigues).

0263-8223/$ - see front matter © 2008 Elsevier Ltd. All rights reserved.
doi:10.1016/j.compstruct.2008.07.025

$$\hat{u}(x) = \sum_{j=1}^{N} c_j \phi_j(x), \quad x \in \mathbb{R}. \tag{1}$$

Traditionally, polynomial basis functions are used, and therefore the above formulation is a univariate one. This leads to the well-known limitation for PS methods: for higher space dimensions their use is pretty much limited to tensor-product grids. In this paper, however, we will use radial basis functions (RBFs) instead of polynomials. This opens up the possibility to work with irregular grids, and on irregular geometries while maintaining a degree of accuracy similar to that obtained with PS methods.

The usual approach to solving PDEs with an RBF collocation method is frequently referred to as *Kansa's method*. For this method one also starts with an expansion of the form (1), now with $\boldsymbol{x} \in \mathbb{R}^s$. However, one then imposes the boundary conditions for the PDE, and forces the PDE and its boundary conditions to be satisfied at a set of collocation points. This leads to a system of linear equations which is solved for the expansion coefficients c_j in (1). Having these coefficients, one can then evaluate the approximate solution $\hat{u}$ at any point $\boldsymbol{x}$ via (1). Thus, with Kansa's collocation method we end up with an approximate solution that is given in terms of a (continuous) function. For more details see, e.g. [42].

Recently, Fornberg et al. (see, e.g. [43,44]) and Schaback [45] showed that certain limiting cases of radial basis functions correspond to polynomial interpolants. This new insight has led to the idea of using pseudospectral methods combined with radial basis functions to solve PDEs (see, e.g. [46–48]). It is this numerical approach that we use for the eigenvalue analysis presented below. For the sake of completeness, we summarize the main ideas of this approach. Consider the linear elliptic PDE problem

$$\mathscr{L}u = f \text{ in } \Omega \tag{2}$$

with Dirichlet boundary condition

$$u = g \text{ on } \Gamma = \partial\Omega. \tag{3}$$

For the pseudospectral approach, we start with an expansion of the form

$$\hat{u}(\boldsymbol{x}) = \sum_{j=1}^{N} c_j \varphi(\|\boldsymbol{x} - \xi_j\|), \quad \boldsymbol{x} \in \Omega \subseteq \mathbb{R}^s, \tag{4}$$

where the points $\xi_j, j = 1, \ldots, N$ are the *centers* of the basis functions $\phi_j = \varphi(\|\cdot - \xi_j\|)$ and φ is one of the usual radial basis functions such as the inverse multiquadric

$$\varphi(r) = \frac{1}{\sqrt{1 + (\varepsilon r)^2}}, \tag{5}$$

the multiquadric

$$\varphi(r) = \sqrt{1 + (\varepsilon r)^2}, \tag{6}$$

the Gaussian

$$\varphi(r) = \mathrm{e}^{-(\varepsilon r)^2}, \tag{7}$$

or a Wendland compactly supported function such as

$$\varphi(r) = (1 - \varepsilon r)_+^8 (32(\varepsilon r)^3 + 25(\varepsilon r)^2 + 8\varepsilon r + 1). \tag{8}$$

The first three of these functions are infinitely differentiable, the Wendland function is six times continuously differentiable. The inverse multiquadric, Gaussian and Wendland functions are positive definite, while the multiquadric is conditionally negative definite. Note that all of our examples contain a positive shape parameter ε. For (inverse) multiquadrics, our notation differs from another popular one for which the shape parameter is denoted by c (not to be confused with the coefficients c_j in the expansion (4)), e.g. $\varphi(r) = 1/\sqrt{r^2 + c^2}$. However, the two formulations are equivalent if we set $\varepsilon = 1/c$. For the Wendland function, the shape parameter determines the size of the support radius (since the $_+$ notation indicates that the function is identically equal to zero outside a sphere of radius r/ε). The advantage of our representation is that all RBFs behave similarly under changes of ε. In particular, $\varepsilon \to 0$ always leads to "flat" basic functions, and it is exactly for this limiting case that the connection to polynomials mentioned at the beginning of this section arises. To be precise, since the compactly supported Wendland functions possess only a limited amount of smoothness they will not be able to provide the full spectral accuracy that polynomials and the other infinitely smooth basis functions are able to. However, the experiments below show that they still provide very high accuracy, and moreover behave in a more stable way than the other basis functions which proved to be beneficial for our eigenvalue analysis.

If we evaluate (4) at a set of *collocation points* $\mathbf{x}_i, i = 1, \ldots, N$, then we get

$$\hat{u}(\boldsymbol{x}_i) = \sum_{j=1}^{N} c_j \varphi(\|\boldsymbol{x}_i - \xi_j\|), \quad i = 1, \ldots, N,$$

or in matrix–vector notation

$$\boldsymbol{u} = A\boldsymbol{c}, \tag{9}$$

where $\boldsymbol{c} = [c_1, \ldots, c_N]^{\mathrm{T}}$ is the coefficient vector, the *evaluation matrix* A has entries $A_{ij} = \varphi(\|\mathbf{x}_i - \xi_j\|)$, and $\boldsymbol{u} = [\hat{u}(\mathbf{x}_1), \ldots, \hat{u}(\boldsymbol{x}_M)]^{\mathrm{T}}$ is a vector of values of the approximate solution at the collocation points.

An important feature of pseudospectral methods is the fact that one usually is content with obtaining an approximation to the solution on a discrete set of grid points $\boldsymbol{x}_i, i = 1, \ldots, N$ instead of at an arbitrary point $\boldsymbol{x}$, as in the popular non-symmetric RBF collocation approach (or Kansa's method). One of several ways to implement the pseudospectral method is via the so-called *differentiation matrices*, i.e., one finds a matrix L such that at the grid points $\mathbf{x}_i$ we have

$$\boldsymbol{u}_{\mathscr{L}} = L\boldsymbol{u}. \tag{10}$$

Here $\boldsymbol{u} = [\hat{u}(\boldsymbol{x}_1), \ldots, \hat{u}(\boldsymbol{x}_N)]^{\mathrm{T}}$ is the vector of values of $\hat{u}$ at the grid points mentioned above, and $\boldsymbol{u}_{\mathscr{L}}$ is the vector of values of the "derivatives" of u at the same points.

Therefore, instead of computing the coefficients $\boldsymbol{c}$ by solving a collocation system – as is done in the standard RBF collocation approach (Kansa's method) – we want to use the differentiation matrix L so that in the end we will have a discrete version of the PDE in the form

$$L\boldsymbol{u} = \boldsymbol{f}, \tag{11}$$

where $\boldsymbol{u}$ is as above and $\boldsymbol{f}$ is the vector of values of the right-hand side f of (2) evaluated at the collocation points.

Since the differential equation for our problem is $\mathscr{L}u = f$, we will apply the differential operator $\mathscr{L}$ to the approximate solution $\hat{u}$ as given by (4). By linearity we get

$$\mathscr{L}\hat{u}(\boldsymbol{x}) = \sum_{j=1}^{N} c_j \mathscr{L}\varphi(\|\boldsymbol{x} - \xi_j\|).$$

Evaluation of this formula at the collocation points $\boldsymbol{x}_i$ yields a system of linear algebraic equations which can be written in matrix–vector notation as

$$L\boldsymbol{u} = A_{\mathscr{L}}\boldsymbol{c}, \tag{12}$$

where $\boldsymbol{u}$ and $\boldsymbol{c}$ are as in (9) above, and the matrix $A_{\mathscr{L}}$ has entries $\mathscr{L}\varphi(\|\mathbf{x} - \xi_j\|)|_{\boldsymbol{x}=\boldsymbol{x}_i}$. The coefficients – which we do not explicitly compute – are given by (9), i.e., $\boldsymbol{c} = A^{-1}\boldsymbol{u}$, so that we formally get

$$L\boldsymbol{u} = A_{\mathscr{L}}A^{-1}\boldsymbol{u}, \tag{13}$$

and we see that the differentiation matrix L is given by $L = A_{\mathscr{L}}A^{-1}$. The name differentiation matrix is due to the fact that L takes the vector $\boldsymbol{u}$ of function values to the vector $L\boldsymbol{u} = \boldsymbol{u}_{\mathscr{L}}$ of "derivative" values (cf. (10)).

Note that this matrix involves inverting the *standard RBF interpolation matrix A* which is known to be nonsingular for all the distributions of centers ξ_j and (coinciding) collocation points $\boldsymbol{x}_i$. This property of A ensures that (at this point in our discussion) we will not run into the problems of possible non-invertibility of the collocation matrix encountered in the popular Kansa method.

Also note that we have not yet enforced the boundary conditions. This, however, is – for the Dirichlet case we are considering here — an absolutely trivial matter. We simply replace those rows of L corresponding to the boundary collocation points (at which we want to enforce the boundary conditions) by standard unit vectors with one in the diagonal position and zeros elsewhere, and replace the corresponding $f(\boldsymbol{x}_k)$ on the right-hand side by $g(\boldsymbol{x}_k)$ (cf. (3)). It is obvious that this works since the resulting product of (boundary) row k of L with the vector $\boldsymbol{u}$ now corresponds to $\hat{u}(\boldsymbol{x}_k) = g(\boldsymbol{x}_k)$ (see, e.g. [41]). One can show that the resulting matrix L_{BC} which also enforces the boundary condition is very closely related to the Kansa matrix, i.e., after a possible permutation of rows we obtain

$$L_{\mathrm{BC}}\boldsymbol{u} = \begin{bmatrix} \widetilde{A}_{\mathscr{L}} \\ \widetilde{A} \end{bmatrix} A^{-1}\boldsymbol{u},$$

where the block matrix on the right-hand side is exactly Kansa's matrix. To obtain a numerical approximation to the solution of the elliptic problem (2) and (3), we actually need to compute

$$\boldsymbol{u} = L_{\mathrm{BC}}^{-1}\begin{bmatrix} \boldsymbol{f} \\ \boldsymbol{g} \end{bmatrix} = \left[\begin{bmatrix} \widetilde{A}_{\mathscr{L}} \\ \widetilde{A} \end{bmatrix} A^{-1}\right]^{-1}\begin{bmatrix} \boldsymbol{f} \\ \boldsymbol{g} \end{bmatrix}, \tag{14}$$

which is the solution of the fully discretized problem (including both the differential operator and the boundary conditions). Assuming invertibility of the two matrix factors gives

$$\boldsymbol{u} = A\begin{bmatrix} \widetilde{A}_{\mathscr{L}} \\ \widetilde{A} \end{bmatrix}^{-1}\begin{bmatrix} \boldsymbol{f} \\ \boldsymbol{g} \end{bmatrix}.$$

This is the same end result as one obtains if the approximate solution for the non-symmetric collocation method (Kansa's method) is evaluated at the collocation points. Note, that in this formulation we now do require invertibility of the Kansa matrix (just as in Kansa's method).

However, as noted above, we do not work with the individual matrices A, $\widetilde{A}_{\mathscr{L}}$, and $\widetilde{A}$, but instead use only the differentiation matrix L_{BC}, so that

$$\boldsymbol{u} = L_{\mathrm{BC}}^{-1}\begin{bmatrix} \boldsymbol{f} \\ \boldsymbol{g} \end{bmatrix}$$

as stated in (14). Moreover, the coefficient vector $\boldsymbol{c}$ is never computed. This can be especially beneficial in the time-dependent problems.

3. Finding an "optimal" shape parameter

As mentioned above, a small shape parameter $\varepsilon \to 0$ will always lead to "flat" basis functions. In fact, the shape parameter ε can be used to influence the accuracy of our numerical method: smaller values of ε generally lead to higher accuracy. However, it is known that there exists a so-called trade-off principle (for infinitely smooth RBFs), i.e., high accuracy can only be achieved at the cost of low numerical stability or vice versa (see, e.g. [49]). This means that it is very difficult to get near the polynomial limit in practice. On the other hand, the optimal value of ε, i.e., the value that produces the smallest error, is usually a positive value [44]. For the Wendland functions we use below, the trade-off principle associated with the variation of ε describes the balance between higher accuracy (for small ε) and numerical efficiency (which results from the increasingly sparse matrices produced by higher values of ϵ). Numerical stability is not so much of an issue with these functions, and that is why we use them here.

A popular strategy for estimating the parameter of a model based on the given data is known as *cross-validation*. In [50], Rippa describes an algorithm that corresponds to a variant of cross-validation known as "*leave-one-out*" *cross-validation* (LOOCV). This method is rather popular in the statistics literature where it is also known as PRESS (predictive residual sum of squares). In this algorithm, an "optimal" value of ε for the RBF interpolation problem is selected by minimizing the error for a fit to the data based on an interpolant for which one of the centers was "left out". This method takes into account the dependence of the error on the data function. Therefore, the predicted "optimal" shape parameter is usually close to the actual optimum value (which we can only find if we know the exact solution of the interpolation problem). We will adopt Rippa's strategy to find the "optimal" shape parameter ε of the basis function used in the RBF-PS method.

First, we explain how the LOOCV method was used in [50] for the interpolation problem. Specifically, if $\mathscr{P}_f^{[k]}$ is the radial basis function interpolant to the data $\{f_1, \ldots, f_{k-1}, f_{k+1}, \ldots, f_N\}$, i.e.,

$$\mathscr{P}_f^{[k]}(\boldsymbol{x}) = \sum_{\substack{j=1 \\ j\neq k}}^{N} c_j^{[k]}\varphi(\|\boldsymbol{x} - \boldsymbol{x}_j\|),$$

and if E_k is the error

$$E_k = f_k - \mathscr{P}_f^{[k]}(\boldsymbol{x}_k),$$

then the quality of the fit is determined by the norm of the vector of errors $E = [E_1, \ldots, E_N]^{\mathrm{T}}$ obtained by removing in turn one of the data points and comparing the resulting fit with the (known) value at the removed point. The norm of E as a function of ε will serve as a *cost function* for the shape parameter.

While a naive implementation of the leave-one-out algorithm is rather expensive (on the order of N^4), Rippa shows that the algorithm can be simplified to a single formula

$$E_k = \frac{c_k}{A_{kk}^{-1}}, \tag{15}$$

where c_k is the kth coefficient in the interpolant $\mathscr{P}_f$ based on the full data set, and A_{kk}^{-1} is the kth diagonal element of the inverse of the corresponding interpolation matrix. This results in $\mathscr{O}(N^3)$ computational complexity. Note that all entries in the error vector E can be computed in a single statement in Matlab if we vectorize the component formula (15) (see line 4 in Program 3.1). In order to find a good value of the shape parameter as quickly as possible, we can use the Matlab function `fminbnd` to find the minimum of the cost function for ε.

Thus, we can implement the cost function in the subroutine `CostEpsilon.m` displayed in Program (3.1). Here, the pseudoinverse of A was used to ensure maximum stability in the solution of the linear system. The cost is computed via the 2-norm.

Program 3.1. `CostEpsilon.m`

```
1 function ceps = CostEpsilon(ep,rbf,r,rhs)
2 A = rbf(ep,r);
3 invA = pinv(A);
4 EF = (invA*rhs)./diag(invA);
5 ceps = norm(EF(:));
```

The calling sequence for `CostEpsilon` will look something like

```
[ep, fval] = fminbnd(@(ep)CostEpsilon(ep, rbf, DM, rhs),
  mine, maxe);
```

where `mine` and `maxe` define the interval to search in for the optimal ε value, and `DM` is a *distance matrix* with entries $\|x_i - \xi_j\|$ used to evaluate the RBF (in the interpolation setting).

The original algorithm in Rippa's paper [50] was intended for the interpolation problem. Therefore, in the context of RBF-PS methods we use a modification of the basic routine `CostEpsilon` which we call `CostEpsilonDRBF` (see Program (3.2) below). Instead of finding an optimal ε for the interpolation problem $Ac = f$, we now need to optimize the choice of ε for the matrix problem (cf. (13))

$$L = A_{\mathscr{L}}A^{-1} \quad \Longleftrightarrow \quad LA = A_{\mathscr{L}} \quad \Longleftrightarrow \quad A^{\mathrm{T}}L^{\mathrm{T}} = (A_{\mathscr{L}})^{\mathrm{T}}.$$

For simplicity, we illustrate the procedure with the first-order derivative $\frac{\partial}{\partial x}$. In this case, we will write A_x instead of the generic $A_{\mathscr{L}}$. Any other differential operator can be implemented analogously. As long as the differential operator is of odd order, we will have to provide both a distance matrix and a *difference matrix*. For differential operators of even order such as the Laplacian, a distance matrix will suffice. For more details see [42].

Program 3.2. `CostEpsilonDRBF.m`

```
% ceps = CostEpsilonDRBF(ep, r, dx, rbf, dxrbf)
% Provides the "cost of epsilon" function for LOOCV %
  optimization
% of shape parameter
% Input: ep, values of shape parameter
% r, dx, distance and difference matrices
% rbf, dxrbf, definition of rbf and its derivative
 1 function ceps = CostEpsilonDRBF(ep, r, dx, rbf, dxrbf)
 2 [m,n] = size(r);
 3 A = rbf(ep,r); % = A^T since A is symmetric
 4 rhs = dxrbf(ep, r, dx)'; % A_x^T
 5 invA = pinv(A);
 6 EF = (invA*rhs)./repmat(diag(invA),1,m);
 7 ceps = norm(EF(:));
```

Note that `CostEpsilonDRBF.m` is very similar to `CostEpsilon.m` (cf. Program (3.1)). Now, however, we compute a right-hand side *matrix* corresponding to the transpose of A_x. Therefore, the denominator – which remains the same for all right-hand sides (see formula (15)) – needs to be cloned on line 6 via the `repmat` command. The cost of ε is now again the (Frobenius) norm of the matrix `EF`. Other measures for the error may also be appropriate. For the standard interpolation setting, Rippa compared the use of the ℓ_1 and ℓ_2 norms (see [50]) and concluded that the ℓ_1 norm yields more accurate "optima". For the RBF-PS problems to be presented here, we have observed very good results with the ℓ_2 (or Frobenius) norm, and therefore that is what is used in line 7 of Program (3.2).

A program that calls `CostEpsilonDRBF` and computes the differentiation matrix (with optimal ε) is given by

Program 3.3. `DRBF.m`

```
% [D,x] = DRBF(N,rbf,dxrbf)
% Computes the differentiation matrix D for 1D derivative
% using Chebyshev points and LOOCV for optimal shape
parameter
% Input: N, number of points -1
% rbf, dxrbf function handles for rbf and its % derivative
% Calls on: DistanceMatrix, DifferenceMatrix
% Requires: CostEpsilonDRBF
 1 function [D,x] = DRBF(N,rbf,dxrbf)
 2 if N==0, D=0; x = 1; return, end
 3 x = cos(pi*(0:N)/N)'; % Chebyshev points
 4 mine = .1; maxe = 10; % Shape parameter interval
 5 r = DistanceMatrix(x,x);
 6 dx = DifferenceMatrix(x,x);
 7a ep = fminbnd(@(ep) CostEpsilonDRBF(ep,r,dx,rbf, dxrbf), ···
 7b      mine, maxe);
 8 fprintf('Using epsilon = % f/n', ep)
 9 A = rbf(ep,r);
10 DA = dxrbf(ep,r,dx);
11 D = DA/A;
```

4. A layerwise theory

The layerwise theory proposed in this paper is based on the assumption of the first-order shear deformation theory in each layer and the imposition of displacement continuity at layer's interfaces. In each layer, the same assumptions as those the first-order plate theories are considered. Due to the size and complexity of the formulation, we restrict the analysis to a three-layer laminate, as shown schematicaly in Fig. 1. However, the present approach is easily extendible to a general laminate.

The displacement field for the middle layer (sometimes known as the core in sandwich laminates) is given as

$$u^{(2)}(x,y,z) = u_0(x,y) + z^{(2)}\theta_x^{(2)}, \tag{16}$$

$$v^{(2)}(x,y,z) = v_0(x,y) + z^{(2)}\theta_y^{(2)}, \tag{17}$$

$$w^{(2)}(x,y,z) = w_0(x,y), \tag{18}$$

where u and v are the in-plane displacements at any point (x,y,z), u_0 and v_0 denote the in-plane displacement of the point $(x,y,0)$ on the midplane, w is the deflection, $\theta_x^{(2)}$ and $\theta_y^{(2)}$ are the rotations of the normals to the midplane about the y and x axes, respectively, for layer 2 (middle layer).

The correspondent displacement field for the upper layer (3) and lower layer (1) is given, respectively, as

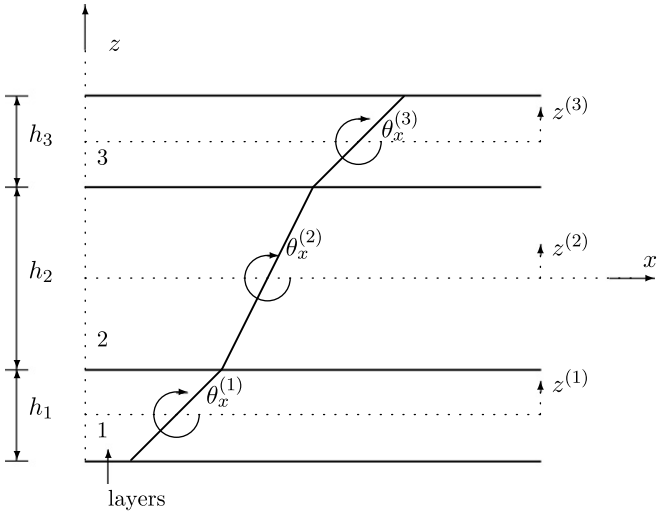

Fig. 1. 1D representation of the layerwise kinematics.

$$u^{(3)}(x,y,z) = u_0(x,y) + \frac{h_2}{2}\theta_x^{(2)} + \frac{h_3}{2}\theta_x^{(3)} + z^{(3)}\theta_x^{(3)}, \tag{19}$$

$$v^{(3)}(x,y,z) = v_0(x,y) + \frac{h_2}{2}\theta_y^{(2)} + \frac{h_3}{2}\theta_y^{(3)} + z^{(3)}\theta_y^{(3)}, \tag{20}$$

$$w^{(3)}(x,y,z) = w_0(x,y), \tag{21}$$

$$u^{(1)}(x,y,z) = u_0(x,y) - \frac{h_2}{2}\theta_x^{(2)} - \frac{h_1}{2}\theta_x^{(1)} + z^{(1)}\theta_x^{(1)}, \tag{22}$$

$$v^{(1)}(x,y,z) = v_0(x,y) - \frac{h_2}{2}\theta_y^{(2)} - \frac{h_1}{2}\theta_y^{(1)} + z^{(1)}\theta_y^{(1)}, \tag{23}$$

$$w^{(1)}(x,y,z) = w_0(x,y), \tag{24}$$

where h_k is the kth layer thickness and $z^{(k)} \in [-h_k/2, h_k/2]$ are the kth layer z-coordinates. Deformations for layer k are given by

$$\begin{Bmatrix} \epsilon_{xx}^{(k)} \\ \epsilon_{yy}^{(k)} \\ \gamma_{xy}^{(k)} \\ \gamma_{xz}^{(k)} \\ \gamma_{yz}^{(k)} \end{Bmatrix} = \begin{Bmatrix} \frac{\partial u^{(k)}}{\partial x} \\ \frac{\partial v^{(k)}}{\partial y} \\ \frac{\partial u^{(k)}}{\partial y} + \frac{\partial v^{(k)}}{\partial x} \\ \frac{\partial u^{(k)}}{\partial z} + \frac{\partial w^{(k)}}{\partial x} \\ \frac{\partial v^{(k)}}{\partial z} + \frac{\partial w^{(k)}}{\partial y} \end{Bmatrix}. \tag{25}$$

Therefore, in-plane deformations can be expressed as

$$\begin{Bmatrix} \epsilon_{xx}^{(k)} \\ \epsilon_{yy}^{(k)} \\ \gamma_{xy}^{(k)} \end{Bmatrix} = \begin{Bmatrix} \epsilon_{xx}^{m(k)} \\ \epsilon_{yy}^{m(k)} \\ \gamma_{xy}^{m(k)} \end{Bmatrix} + z^{(k)} \begin{Bmatrix} \epsilon_{xx}^{f(k)} \\ \epsilon_{yy}^{f(k)} \\ \gamma_{xy}^{f(k)} \end{Bmatrix} + \begin{Bmatrix} \epsilon_{xx}^{mf(k)} \\ \epsilon_{yy}^{mf(k)} \\ \gamma_{xy}^{mf(k)} \end{Bmatrix}, \tag{26}$$

and shear deformations as

$$\begin{Bmatrix} \gamma_{xz}^{(k)} \\ \gamma_{yz}^{(k)} \end{Bmatrix} = \begin{Bmatrix} \frac{\partial w_0}{\partial x} + \theta_x^{(k)} \\ \frac{\partial w_0}{\partial y} + \theta_y^{(k)} \end{Bmatrix}. \tag{27}$$

The membrane components are given by

$$\begin{Bmatrix} \epsilon_{xx}^{m(k)} \\ \epsilon_{yy}^{m(k)} \\ \gamma_{xy}^{m(k)} \end{Bmatrix} = \begin{Bmatrix} \frac{\partial u_0}{\partial x} \\ \frac{\partial v_0}{\partial y} \\ \frac{\partial u_0}{\partial y} + \frac{\partial v_0}{\partial x} \end{Bmatrix}. \tag{28}$$

The bending components can be expressed as

$$\begin{Bmatrix} \epsilon_{xx}^{f(k)} \\ \epsilon_{yy}^{f(k)} \\ \gamma_{xy}^{f(k)} \end{Bmatrix} = \begin{Bmatrix} \frac{\partial \theta_x^{(k)}}{\partial x} \\ \frac{\partial \theta_y^{(k)}}{\partial y} \\ \frac{\partial \theta_x^{(k)}}{\partial y} + \frac{\partial \theta_y^{(k)}}{\partial x} \end{Bmatrix}, \tag{29}$$

and the membrane-bending coupling components for layers 2, 3 and 1 are, respectively, given as

$$\begin{Bmatrix} \epsilon_{xx}^{mf(2)} \\ \epsilon_{yy}^{mf(2)} \\ \gamma_{xy}^{mf(2)} \end{Bmatrix} = \begin{Bmatrix} 0 \\ 0 \\ 0 \end{Bmatrix}, \tag{30}$$

$$\begin{Bmatrix} \epsilon_{xx}^{mf(3)} \\ \epsilon_{yy}^{mf(3)} \\ \gamma_{xy}^{mf(3)} \end{Bmatrix} = \begin{Bmatrix} \frac{h_2}{2}\frac{\partial \theta_x^{(2)}}{\partial x} + \frac{h_3}{2}\frac{\partial \theta_x^{(3)}}{\partial x} \\ \frac{h_2}{2}\frac{\partial \theta_y^{(2)}}{\partial y} + \frac{h_3}{2}\frac{\partial \theta_y^{(3)}}{\partial y} \\ \frac{h_2}{2}\left(\frac{\partial \theta_x^{(2)}}{\partial y} + \frac{\partial \theta_y^{(2)}}{\partial x}\right) + \frac{h_3}{2}\left(\frac{\partial \theta_x^{(3)}}{\partial y} + \frac{\partial \theta_y^{(3)}}{\partial x}\right) \end{Bmatrix}, \tag{31}$$

$$\begin{Bmatrix} \epsilon_{xx}^{mf(1)} \\ \epsilon_{yy}^{mf(1)} \\ \gamma_{xy}^{mf(1)} \end{Bmatrix} = \begin{Bmatrix} -\frac{h_2}{2}\frac{\partial \theta_x^{(2)}}{\partial x} - \frac{h_1}{2}\frac{\partial \theta_x^{(1)}}{\partial x} \\ -\frac{h_2}{2}\frac{\partial \theta_y^{(2)}}{\partial y} - \frac{h_1}{2}\frac{\partial \theta_y^{(1)}}{\partial y} \\ -\frac{h_2}{2}\left(\frac{\partial \theta_x^{(2)}}{\partial y} + \frac{\partial \theta_y^{(2)}}{\partial x}\right) - \frac{h_1}{2}\left(\frac{\partial \theta_x^{(1)}}{\partial y} + \frac{\partial \theta_y^{(1)}}{\partial x}\right) \end{Bmatrix}. \tag{32}$$

Setting $\sigma_z^{(k)} = 0$ for each orthotropic layer, solving the equation for $\epsilon_{zz}^{(k)}$ and substituting for $\epsilon_{zz}^{(k)}$ in the remaining equations, the stress–strain relations in the fiber local coordinate system can be expressed as

$$\begin{Bmatrix} \sigma_1^{(k)} \\ \sigma_2^{(k)} \\ \tau_{12}^{(k)} \\ \tau_{23}^{(k)} \\ \tau_{31}^{(k)} \end{Bmatrix} = \begin{bmatrix} Q_{11} & Q_{12} & 0 & 0 & 0 \\ Q_{12} & Q_{22} & 0 & 0 & 0 \\ 0 & 0 & Q_{33} & 0 & 0 \\ 0 & 0 & 0 & Q_{44} & 0 \\ 0 & 0 & 0 & 0 & Q_{55} \end{bmatrix}^{(k)} \begin{Bmatrix} \varepsilon_1^{(k)} \\ \varepsilon_2^{(k)} \\ \gamma_{12}^{(k)} \\ \gamma_{23}^{(k)} \\ \gamma_{31}^{(k)} \end{Bmatrix}, \tag{33}$$

where subscripts 1 and 2 are, respectively, the fiber and the normal to fiber in-plane directions, 3 is the direction normal to the plate, and the reduced stiffness components, $Q_{ij}^{(k)}$, are given by

$$Q_{11}^{(k)} = \frac{E_1^{(k)}}{1 - \nu_{12}^{(k)}\nu_{21}^{(k)}}, \quad Q_{22}^{(k)} = \frac{E_2^{(k)}}{1 - \nu_{12}^{(k)}\nu_{21}^{(k)}}, \quad Q_{12}^{(k)} = \nu_{21}^{(k)} Q_{11}^{(k)},$$
$$Q_{33}^{(k)} = G_{12}^{(k)}, \quad Q_{44}^{(k)} = G_{23}^{(k)}, \quad Q_{55}^{(k)} = G_{31}^{(k)},$$
$$\nu_{21}^{(k)} = \nu_{12}^{(k)} \frac{E_2^{(k)}}{E_1^{(k)}},$$

in which $E_1^{(k)}, E_2^{(k)}, \nu_{12}^{(k)}, G_{12}^{(k)}, G_{23}^{(k)}$ and $G_{31}^{(k)}$ are material properties of lamina k. By performing coordinate transformations, the stress–strain relations in the global x–y–z coordinate system can be obtained as

$$\begin{Bmatrix} \sigma_{xx}^{(k)} \\ \sigma_{yy}^{(k)} \\ \tau_{xy}^{(k)} \\ \tau_{yz}^{(k)} \\ \tau_{zx}^{(k)} \end{Bmatrix} = \begin{bmatrix} \overline{Q}_{11}^{(k)} & \overline{Q}_{12}^{(k)} & \overline{Q}_{16}^{(k)} & 0 & 0 \\ \overline{Q}_{12}^{(k)} & \overline{Q}_{22}^{(k)} & \overline{Q}_{26}^{(k)} & 0 & 0 \\ \overline{Q}_{16}^{(k)} & \overline{Q}_{26}^{(k)} & \overline{Q}_{66}^{(k)} & 0 & 0 \\ 0 & 0 & 0 & \overline{Q}_{44}^{(k)} & \overline{Q}_{45}^{(k)} \\ 0 & 0 & 0 & \overline{Q}_{45}^{(k)} & \overline{Q}_{55}^{(k)} \end{bmatrix} \begin{Bmatrix} \varepsilon_{xx}^{(k)} \\ \varepsilon_{yy}^{(k)} \\ \gamma_{xy}^{(k)} \\ \gamma_{yz}^{(k)} \\ \gamma_{zx}^{(k)} \end{Bmatrix}. \tag{34}$$

By considering α as the angle between x-axis and 1-axis, with 1-axis being the first principal material axis, connected usually with fiber direction, the components $\overline{Q}_{ij}^{(k)}$ can be calculated by coordinate transformation, as in [11].

We note that the displacement field given by equations (16) through (24) satisfies the continuity of displacements across an interface between two adjoining layers. However, stresses resulting from them and the constitutive relations (34) may not satisfy the continuity of tractions across these interfaces. Errors introduced by this approximation are generally small, as will be verified by the good agreement between the presently computed results and those obtained from the analytical solution of the problem.

The equations of motion of this layerwise theory are derived from the principle of virtual displacements. In this work, only symmetric laminates are considered, therefore u_0, v_0 and the related stress resultants can be discarded.

The virtual strain energy (δU), the virtual kinetic energy (δK) and the virtual work done by applied forces (δV), assuming a three-layer laminate, are given by

$$\begin{aligned} \delta U &= \int_{\Omega_0} \sum_{k=1}^{3} \left\{ \int_{-h_k/2}^{h_k/2} \left[\sigma_{xx}(z\delta\epsilon_{xx}^{f(k)} + \delta\epsilon_{xx}^{mf(k)}) + \sigma_{yy}(z\delta\epsilon_{yy}^{f(k)} + \delta\epsilon_{yy}^{mf(k)}) \right.\right. \\ &\quad \left.\left. + \tau_{xy}(z\delta\gamma_{xy}^{f(k)} + \delta\gamma_{xy}^{mf(k)}) + \tau_{xz}\delta\gamma_{xz}^{(k)} + \tau_{yz}\delta\gamma_{yz}^{(k)} \right] \mathrm{d}z \right\} \mathrm{d}x\,\mathrm{d}y \Big| \\ &= \int_{\Omega_0} \sum_{k=1}^{3} \left(N_{xx}^{(k)}\delta\epsilon_{xx}^{mf(k)} + M_{xx}^{(k)}\delta\epsilon_{xx}^{f(k)} + N_{yy}^{(k)}\delta\epsilon_{yy}^{mf(k)} + M_{yy}^{(k)}\delta\epsilon_{yy}^{f(k)} \right. \\ &\quad \left. + N_{xy}^{(k)}\delta\gamma_{xy}^{mf(k)} + M_{xy}^{(k)}\delta\gamma_{xy}^{f(k)} + Q_x^{(k)}\delta\gamma_{xz}^{(k)} + Q_y^{(k)}\delta\gamma_{yz}^{(k)} \right) \mathrm{d}x\,\mathrm{d}y, \end{aligned} \tag{35}$$

$$\delta K = \int_{\Omega_0} \sum_{k=1}^{3} \int_{-h_k/2}^{h_k/2} \rho^{(k)} \left(\dot{u}^k \delta\dot{u}^k + \dot{\mathbf{v}}^k \delta\dot{\mathbf{v}}^k + \dot{\mathbf{w}}^k \delta\dot{\mathbf{w}}^k \right) \mathrm{d}z\,\mathrm{d}x\,\mathrm{d}y, \tag{36}$$

and

$$\delta V = -\int_{\Omega_0} q\delta w_0 \,\mathrm{d}x\,\mathrm{d}y, \tag{37}$$

where Ω_0 denotes the midplane of the laminate, q is the external distributed load and

$$\begin{Bmatrix} N^{(k)}_{\alpha\beta} \\ M^{(k)}_{\alpha\beta} \end{Bmatrix} = \int_{-h_k/2}^{h_k/2} \sigma^{(k)}_{\alpha\beta} \begin{Bmatrix} 1 \\ z \end{Bmatrix} \mathrm{d}z_k, \tag{38}$$

$$Q^{(k)}_{\alpha} = \int_{-h_k/2}^{h_k/2} \tau^{(k)}_{\alpha z} \,\mathrm{d}z_k, \tag{39}$$

where α, β take the symbols x, y.

Substituting for $\delta U, \delta K, \delta V$ into the virtual work statement, noting that the virtual strains can be expressed in terms of the generalized displacements, integrating by parts to relieve from any derivatives of the generalized displacements and using the fundamental lemma of the calculus of variations, we obtain the equations of motion [11] with respect to 7 degrees of freedom $(w_0, \theta^{(1)}_x, \theta^{(1)}_y, \theta^{(2)}_x, \theta^{(2)}_y, \theta^{(3)}_x, \theta^{(3)}_y)$ (see Fig. 1):

$$\delta w_0 : \sum_{k=1}^{3} \left(\frac{\partial Q^{(k)}_x}{\partial x} + \frac{\partial Q^{(k)}_y}{\partial y} \right) - q = \sum_{k=1}^{3} I^{(k)}_0 \ddot{w}_0, \tag{40}$$

$$\begin{aligned} \delta\theta^{(1)}_x : {} & \frac{h_1}{2}\frac{\partial N^{(1)}_{xx}}{\partial x} - \frac{\partial M^{(1)}_{xx}}{\partial x} + \frac{h_1}{2}\frac{\partial N^{(1)}_{xy}}{\partial y} - \frac{\partial M^{(1)}_{xy}}{\partial y} + Q^{(1)}_x \\ & = I^{(1)}_0 \left(\frac{h_1 h_2}{4}\ddot{\theta}_{x2} + \frac{h_1^2}{4}\ddot{\theta}_{x1} \right) + I^{(1)}_2 \ddot{\theta}_{x1}, \end{aligned} \tag{41}$$

$$\begin{aligned} \delta\theta^{(1)}_y : {} & \frac{h_1}{2}\frac{\partial N^{(1)}_{yy}}{\partial y} - \frac{\partial M^{(1)}_{yy}}{\partial y} + \frac{h_1}{2}\frac{\partial N^{(1)}_{xy}}{\partial x} - \frac{\partial M^{(1)}_{xy}}{\partial x} + Q^{(1)}_y \\ & = I^{(1)}_0 \left(\frac{h_1 h_2}{4}\ddot{\theta}_{y2} + \frac{h_1^2}{4}\ddot{\theta}_{y1} \right) + I^{(1)}_2 \ddot{\theta}_{y1}, \end{aligned} \tag{42}$$

$$\begin{aligned} \delta\theta^{(2)}_x : {} & \frac{h_2}{2}\frac{\partial N^{(1)}_{xx}}{\partial x} - \frac{h_2}{2}\frac{\partial N^{(3)}_{xx}}{\partial x} - \frac{\partial M^{(2)}_{xx}}{\partial x} + \frac{h_2}{2}\frac{\partial N^{(1)}_{xy}}{\partial y} - \frac{h_2}{2}\frac{\partial N^{(3)}_{xy}}{\partial y} \\ & - \frac{\partial M^{(2)}_{xy}}{\partial y} + Q^{(2)}_x \\ & = I^{(1)}_0 \left(\frac{h_2^2}{4}\ddot{\theta}_{x2} + \frac{h_1 h_2}{4}\ddot{\theta}_{x1} \right) + I^{(3)}_0 \left(\frac{h_2^2}{4}\ddot{\theta}_{x2} + \frac{h_2 h_3}{4}\ddot{\theta}_{x3} \right) \\ & + I^{(2)}_2 \ddot{\theta}_{x2}, \end{aligned} \tag{43}$$

$$\begin{aligned} \delta\theta^{(2)}_y : {} & \frac{h_2}{2}\frac{\partial N^{(1)}_{yy}}{\partial y} - \frac{h_2}{2}\frac{\partial N^{(3)}_{yy}}{\partial y} - \frac{\partial M^{(2)}_{yy}}{\partial y} + \frac{h_2}{2}\frac{\partial N^{(1)}_{xy}}{\partial x} - \frac{h_2}{2}\frac{\partial N^{(3)}_{xy}}{\partial x} \\ & - \frac{\partial M^{(2)}_{xy}}{\partial x} + Q^{(2)}_y \\ & = I^{(1)}_0 \left(\frac{h_2^2}{4}\ddot{\theta}_{y2} + \frac{h_1 h_2}{4}\ddot{\theta}_{y1} \right) + I^{(3)}_0 \left(\frac{h_2^2}{4}\ddot{\theta}_{y2} + \frac{h_2 h_3}{4}\ddot{\theta}_{y3} \right) \\ & + I^{(2)}_2 \ddot{\theta}_{y2}, \end{aligned} \tag{44}$$

$$\begin{aligned} \delta\theta^{(3)}_x : {} & -\frac{h_3}{2}\frac{\partial N^{(3)}_{xx}}{\partial x} - \frac{\partial M^{(3)}_{xx}}{\partial x} - \frac{h_3}{2}\frac{\partial N^{(3)}_{xy}}{\partial y} - \frac{\partial M^{(3)}_{xy}}{\partial y} + Q^{(3)}_x \\ & = I^{(3)}_0 \left(\frac{h_2 h_3}{4}\ddot{\theta}_{x2} + \frac{h_3^2}{4}\ddot{\theta}_{x3} \right) + I^{(3)}_2 \ddot{\theta}_{x3}, \end{aligned} \tag{45}$$

$$\begin{aligned} \delta\theta^{(3)}_y : {} & -\frac{h_3}{2}\frac{\partial N^{(3)}_{yy}}{\partial y} - \frac{\partial M^{(3)}_{yy}}{\partial y} - \frac{h_3}{2}\frac{\partial N^{(3)}_{xy}}{\partial x} - \frac{\partial M^{(3)}_{xy}}{\partial x} + Q^{(3)}_y \\ & = I^{(3)}_0 \left(\frac{h_2 h_3}{4}\ddot{\theta}_{y2} + \frac{h_3^2}{4}\ddot{\theta}_{y3} \right) + I^{(3)}_2 \ddot{\theta}_{y3}, \end{aligned} \tag{46}$$

where

$$\left(I^{(k)}_0, I^{(k)}_2 \right) = \int_{-h_k/2}^{h_k/2} \rho^{(k)}(1, z^2)\,\mathrm{d}z \tag{47}$$

ρ being the mass density of the material and h_k the thickness of the kth layer.

The equations of motion can be written in terms of the displacements by substituting for strains and stress resultants into the previous equations. As an example, the first equation is replaced by

$$\begin{aligned} \delta w_0 : {} & \sum_{k=1}^{3} h_k \left(\overline{Q}^{(k)}_{55} \left(\frac{\partial^2 w_0}{\partial x^2} + \frac{\partial \theta^{(k)}_x}{\partial x} \right) + \overline{Q}^{(k)}_{44} \left(\frac{\partial^2 w_0}{\partial y^2} + \frac{\partial \theta^{(k)}_y}{\partial y} \right) \right) - q \\ & = \sum_{k=1}^{3} I^{(k)}_0 \ddot{w}_0. \end{aligned} \tag{48}$$

5. Free vibration analysis

For free vibration problems, we assume harmonic solution in terms of displacements $w_0, \theta^{(k)}_x, \theta^{(k)}_y$ in the form

$$w_0(x, y, t) = W(w, y)\mathrm{e}^{\mathrm{i}\omega t}, \tag{49}$$

$$\theta^{(k)}_x(x, y, t) = \Psi^{(k)}_x(w, y)\mathrm{e}^{\mathrm{i}\omega t}, \tag{50}$$

$$\theta^{(k)}_y(x, y, t) = \Psi^{(k)}_y(w, y)\mathrm{e}^{\mathrm{i}\omega t}, \tag{51}$$

where ω is the frequency of natural vibration. Removing the external force q and substituting the harmonic expansion into equations of motion, we obtain Eq. (48) in terms of the amplitudes $W, \Psi^{(k)}_x, \Psi^{(k)}_y$, where $k = 1, 2, 3$

$$\begin{aligned} \delta w_0 : {} & \sum_{k=1}^{3} h_k \left(\overline{Q}^{(k)}_{55} \left(\frac{\partial^2 w_0}{\partial x^2} + \frac{\partial \theta^{(k)}_x}{\partial x} \right) + \overline{Q}^{(k)}_{44} \left(\frac{\partial^2 w_0}{\partial y^2} + \frac{\partial \theta^{(k)}_y}{\partial y} \right) \right) \\ & = -\sum_{k=1}^{3} I^{(k)}_0 \omega^2 W. \end{aligned} \tag{52}$$

The remaining equations of motion are dealt with in a similar way.

6. Interpolation of differential equations of motion and boundary conditions by radial basis functions

The equations of motion are now interpolated by radial basis functions, for each node i. For example, Eq. (52) is expressed as

$$\begin{aligned} \delta w_0 : {} & \sum_{k=1}^{3} h_k \left(\overline{Q}^{(k)}_{55} \left(\sum_{j=1}^{N} a^w_j \frac{\partial^2 \varphi_j}{\partial x^2} + \sum_{j=1}^{N} a^{\theta^{(k)}_x}_j \frac{\partial \varphi_j}{\partial x} \right) \right. \\ & \left. + \overline{Q}^{(k)}_{44} \left(\sum_{j=1}^{N} a^w_j \frac{\partial^2 \varphi_j}{\partial y^2} + \sum_{j=1}^{N} a^{\theta^{(k)}_y}_j \frac{\partial \varphi_j}{\partial y} \right) \right) = -\sum_{k=1}^{3} I^{(k)}_0 \omega^2 \sum_{j=1}^{N} a^w_j \varphi_j, \end{aligned} \tag{53}$$

where φ_j was defined before and N represents the total number of discretization points.

The other six equations are interpolated in a similar way. The vector of unknowns is now composed of the interpolation parameters a_j, for $w_0, \theta^{(1)}_x, \theta^{(1)}_y, \theta^{(2)}_x, \theta^{(2)}_y, \theta^{(3)}_x, \theta^{(3)}_y$, respectively.

For each boundary node, the RBF interpolation is also quite simple. As an example, a simply-supported condition at $x = \beta$ edge with outward normal direction α imposes seven boundary conditions as follows:

$$w_0 = 0, \tag{54}$$

$$M^{(k)}_{\alpha\alpha} = 0, \tag{55}$$

$$\theta^{(k)}_{\beta} = 0. \tag{56}$$

These conditions are equivalent to

$$w_0 = 0, \tag{57}$$

$$\delta\theta_x^{(1)}\left(-\frac{h_1}{2}N_{xx}^{(1)} - \frac{h_1}{2}N_{xy}^{(1)} + M_{xx}^{(1)}\right) + \delta\theta_x^{(2)}\left(-\frac{h_2}{2}N_{xx}^{(1)} + \frac{h_2}{2}N_{xx}^{(3)} - \frac{h_2}{2}N_{xy}^{(1)} + \frac{h_2}{2}N_{xy}^{(3)} + M_{xx}^{(2)}\right) + \delta\theta_x^{(3)}\left(\frac{h_3}{2}N_{xx}^{(3)} + M_{xx}^{(3)}\right) = 0, \tag{58}$$

$$\theta_\beta^{(k)} = 0. \tag{59}$$

The RBF interpolation of boundary equations leads to a change in the global equations system. For each node i where the equations are valid, the following equations are imposed. For example, Eq. (57) is interpolated as

$$\sum_{j=1}^{N} a_j^w \varphi_j = 0, \tag{60}$$

where N represents the total number of grid points. The other boundary conditions are interpolated in the same way.

7. Numerical examples

In all the following examples, a Chebyshev grid was used. The radial basis function used was a compact support Wendland function in the form

$$\varphi(r) = (1-\varepsilon r)_+^8(32(\varepsilon r)^3 + 25(\varepsilon r)^2 + 8\varepsilon r + 1), \tag{61}$$

where ϵ is the shape parameter and r an Euclidean distance. For all cases, the optimum factor seems to be only dependent on the number of nodes. Up to 17×17 nodes, $\epsilon = 0.1$, while for $21\times 21, \epsilon = 0.104$.

7.1. Three layer square sandwich plate in bending, under uniform load

A simply supported sandwich square plate, under a uniform transverse load is considered. This is the classical sandwich example of Srinivas [51].

The material properties of the sandwich core are expressed in the stiffness matrix, $\overline{Q}_{\text{core}}$ as

$$\overline{Q}_{\text{core}} = \begin{bmatrix} 0.999781 & 0.231192 & 0 & 0 & 0 \\ 0.231192 & 0.524886 & 0 & 0 & 0 \\ 0 & 0 & 0.262931 & 0 & 0 \\ 0 & 0 & 0 & 0.266810 & 0 \\ 0 & 0 & 0 & 0 & 0.159914 \end{bmatrix}.$$

The material properties of the face sheets are related to those of the core material properties by a factor R as

$$\overline{Q}_{\text{skin}} = R\overline{Q}_{\text{core}}.$$

Transverse displacement and stresses are normalized as

$$\overline{w} = w(a/2, a/2, 0)\frac{0.999781}{hq},$$

$$\overline{\sigma}_x^1 = \frac{\sigma_x^{(1)}(a/2,a/2,-h/2)}{q}; \quad \overline{\sigma}_x^2 = \frac{\sigma_x^{(1)}(a/2,a/2,-2h/5)}{q}; \quad \overline{\sigma}_x^3 = \frac{\sigma_x^{(2)}(a/2,a/2,-2h/5)}{q},$$

$$\overline{\sigma}_y^1 = \frac{\sigma_y^{(1)}(a/2,a/2,-h/2)}{q}; \quad \overline{\sigma}_y^2 = \frac{\sigma_y^{(1)}(a/2,a/2,-2h/5)}{q}; \quad \overline{\sigma}_y^3 = \frac{\sigma_y^{(2)}(a/2,a/2,-2h/5)}{q},$$

$$\overline{\tau}_{xz}^1 = \frac{\tau_{xz}^{(2)}(0,a/2,0)}{q}; \quad \overline{\tau}_{xz}^2 = \frac{\tau_{xz}^{(2)}(0,a/2,-2h/5)}{q}.$$

Transverse displacement and stresses for a sandwich plate are indicated in Tables 1–3 and compared with those from various formulations. These formulations provide very good results both for displacement and for stresses. It can be seen that the present formulation achieves very good results for all cases, without the use of shear correction factors. The FSDT and HSDT results of Pandya and Kant [52] cannot match our formulation for sandwich laminates where skin properties are quite different than core properties, which is the typical industrial case. So for $R = 15$ or larger this formulation should be adopted. The work of Ferreira and Barbosa in laminated shell finite elements [53] and multiquadrics [35] using the first-order shear deformation approach is also compared. The results are as good or better than results from the present formulation. However, this was achieved by a shear correction procedure [35] that is dependent on some assumptions that may not be general, although quite good for all the tested cases so far. The present layerwise formulation is better than the third-order formulation presented by Ferreira et al. [37], particularly in sandwich plates with skin properties much higher than core properties.

7.2. Three layer (0/90/0) square cross-ply laminated plate under sinusoidal load

A simply supported square laminated plate of side a and thickness h is composed of four equal layers oriented at [0°/90°/90°/0°]. The plate is subjected to a sinusoidal vertical pressure of the form:

$$p_z = P\sin\left(\frac{\pi x}{a}\right)\sin\left(\frac{\pi y}{a}\right),$$

with the origin of the coordinate system located at the lower left corner on the midplane.

The material properties are given by

$$E_1 = 25.0E_2 \quad G_{12} = G_{13} = 0.5E_2 \quad G_{23} = 0.2E_2 \quad \nu_{12} = 0.25.$$

In Table 4, results from the present method are compared with those from a finite strip formulation by Akhras [54,55] who used three strips, an analytical solution by Reddy [56] using a higher-order formulation and the exact three-dimensional solution by Pagano [57]. The present solution is also compared with another higher-order solution [37]. The in-plane displacements, the transverse displacements, the normal stresses and the in-plane and the transverse shear stresses are presented in normalized form as

$$\overline{w} = \frac{10^2 w_{\max} h^3 E_2}{Pa^4}, \quad \overline{\sigma}_{xx} = \frac{\sigma_{xx}h^2}{Pa^2}, \quad \overline{\sigma}_{yy} = \frac{\sigma_{yy}h^2}{Pa^2}, \quad \overline{\tau}_{zx} = \frac{\tau_{zx}h}{Pa},$$

$$\overline{\tau}_{xy} = \frac{\tau_{xy}h^2}{Pa^2}.$$

The transverse shear stresses are calculated directly from the constitutive equations. This is a feature of this theory, whereas other equivalent single layer theories such as Reddy's third-order theory need to calculate transverse shear stresses using the equilibrium equations.

Table 1
Square laminated plate under uniform load-$R = 5$

Method	$\overline{w}$	$\overline{\sigma}_x^1$	$\overline{\sigma}_x^2$	$\overline{\sigma}_x^3$	$\overline{\sigma}_y^1$	$\overline{\sigma}_y^2$	$\overline{\sigma}_y^3$	$\overline{\tau}_{xz}^1$	$\overline{\tau}_{xz}^2$
HSDT [52]	256.13	62.38	46.91	9.382	38.93	30.33	6.065	3.089	2.566
FSDT [52]	236.10	61.87	49.50	9.899	36.65	29.32	5.864	3.313	2.444
CLT	216.94	61.141	48.623	9.783	36.622	29.297	5.860	4.5899	3.386
Ferreira [53]	258.74	59.21	45.61	9.122	37.88	29.59	5.918	3.593	3.593
Ferreira ($N = 15$) [35]	257.38	58.725	46.980	9.396	37.643	27.714	4.906	3.848	2.839
exact [51]	258.97	60.353	46.623	9.340	38.491	30.097	6.161	4.3641	3.2675
HSDT [37] ($N = 11$)	253.6710	59.6447	46.4292	9.2858	38.0694	29.9313	5.9863	3.8449	1.9650
HSDT [37] ($N = 15$)	256.2387	60.1834	46.8581	9.3716	38.3592	30.1642	6.0328	4.2768	2.2227
HSDT [37] ($N = 21$)	257.1100	60.3660	47.0028	9.4006	38.4563	30.2420	6.0484	4.5481	2.3910
Present ($N = 11$)($\epsilon = 0.1$)	258.2812	60.7292	46.7031	9.3406	39.0424	30.4338	6.0868	4.1061	2.2934
Present ($N = 15$)($\epsilon = 0.1$)	258.1813	60.2973	46.4641	9.2928	38.5549	30.1141	6.0228	4.0961	2.1262
Present ($N = 21$)($\epsilon = 0.104$)	258.1795	60.0626	46.3926	9.2785	38.3644	30.0294	6.0059	4.0950	2.0418

Table 2
Square laminated plate under uniform load-$R = 10$

Method	$\overline{w}$	$\overline{\sigma}_x^1$	$\overline{\sigma}_x^2$	$\overline{\sigma}_x^3$	$\overline{\sigma}_y^1$	$\overline{\sigma}_y^2$	$\overline{\sigma}_y^3$	$\overline{\tau}_{xz}^1$	$\overline{\tau}_{xz}^2$
HSDT [52]	152.33	64.65	51.31	5.131	42.83	33.97	3.397	3.147	2.587
FSDT [52]	131.095	67.80	54.24	4.424	40.10	32.08	3.208	3.152	2.676
CLT	118.87	65.332	48.857	5.356	40.099	32.079	3.208	4.3666	3.7075
Ferreira [53]	159.402	64.16	47.72	4.772	42.970	42.900	3.290	3.518	3.518
Ferreira ($N = 15$) [35]	158.55	62.723	50.16	5.01	42.565	34.052	3.400	3.596	3.053
Exact [51]	159.38	65.332	48.857	4.903	43.566	33.413	3.500	4.0959	3.5154
Third-order [37] ($N = 11$)	153.0084	64.7415	49.4716	4.9472	42.8860	33.3524	3.3352	2.7780	1.8207
Third-order [37] ($N = 15$)	154.2490	65.2223	49.8488	4.9849	43.1521	33.5663	3.3566	3.1925	2.1360
Third-order [37] ($N = 21$)	154.6581	65.3809	49.9729	4.9973	43.2401	33.6366	3.3637	3.5280	2.3984
Present ($N = 11$)($\epsilon = 0.1$)	159.0260	66.0311	48.7610	4.8761	44.2945	33.6994	3.3699	3.9550	2.5388
Present ($N = 15$)($\epsilon = 0.1$)	158.9237	65.3861	48.5365	4.8537	43.7554	33.4149	3.3415	3.9842	2.4860
Present ($N = 21$)($\epsilon = 0.104$)	158.9117	64.9927	48.6009	4.8601	43.4907	33.4089	3.3409	3.9803	2.3325

Table 3
Square laminated plate under uniform load-$R = 15$

Method	$\overline{w}$	$\overline{\sigma}_x^1$	$\overline{\sigma}_x^2$	$\overline{\sigma}_x^3$	$\overline{\sigma}_y^1$	$\overline{\sigma}_y^2$	$\overline{\sigma}_y^3$	$\overline{\tau}_{xz}^1$	$\overline{\tau}_{xz}^2$
HSDT [52]	110.43	66.62	51.97	3.465	44.92	35.41	2.361	3.035	2.691
FSDT [52]	90.85	70.04	56.03	3.753	41.39	33.11	2.208	3.091	2.764
CLT	81.768	69.135	55.308	3.687	41.410	33.128	2.209	4.2825	3.8287
Ferreira [53]	121.821	65.650	47.09	3.140	45.850	34.420	2.294	3.466	3.466
Ferreira ($N = 15$) [35]	121.184	63.214	50.571	3.371	45.055	36.044	2.400	3.466	3.099
Exact [51]	121.72	66.787	48.299	3.238	46.424	34.955	2.494	3.9638	3.5768
Third-order [37] ($N = 11$)	113.5941	66.3646	49.8957	3.3264	45.2979	34.9096	2.3273	2.1686	1.5578
Third-order [37] ($N = 15$)	114.3874	66.7830	50.2175	3.3478	45.5427	35.1057	2.3404	2.6115	1.9271
Third-order [37] ($N = 21$)	114.6442	66.9196	50.3230	3.3549	45.6229	35.1696	2.3446	3.0213	2.2750
Present ($N = 11$)($\epsilon = 0.1$)	121.3949	67.6166	47.9685	3.1979	47.1146	35.0756	2.3384	3.8332	2.5772
Present ($N = 15$)($\epsilon = 0.1$)	121.3381	66.8559	47.8129	3.1875	46.6254	34.8805	2.3254	3.9062	2.6885
Present ($N = 21$)($\epsilon = 0.104$)	121.3474	66.4362	48.0104	3.2007	46.3849	34.9650	2.3310	3.9024	2.4811

The present layerwise theory discretized with multiquadrics presents better results than the previous results by Ferreira et al. [37]. Results for transverse displacements and stresses are better than the results of Akhras and Reddy when compared with the exact solutions.

7.3. Natural frequencies of isotropic clamped square plates

The length of the isotropic plate is a and two thickness-to-side ratios $h/a = 0.01$ and 0.1 are considered. A non-dimensional frequency parameter is defined as

$$\bar{\lambda} = \lambda_{mn} a \sqrt{\frac{\rho}{G}},$$

where λ is the frequency, ρ is the mass density per unit volume, G is the shear modulus and $G = E/(2(1+\nu))$, E Young's modulus and $\nu = 0.3$ the Poisson ratio. The subscripts m and n denote the number of half-waves in the mode shapes in the x and y directions, respectively.

The plates are clamped at all boundary edges. The first eight modes of vibration for both plates are calculated. Two cases of thickness-to-side ratio $h/a = 0.01$ and 0.1 are considered. The comparison of frequency parameters with the Rayleigh–Ritz solutions [58] and results by Liew et al. [59], using a reproducing kernel particle approximation, for each plate is listed in Tables 5 and 6. Excellent agreement is obtained, in fact our solution is closer to the Rayleigh–Ritz solutions than that of Liew. In Figs. 2 and 3 the first eight mode shapes of the CCCC plate ($h/a = 0.1$) are presented. In Figs. 4 and 5 the first eight mode shapes for $h/a = 0.01$ are shown. The corresponding 3D views are illustrated in Figs. 6 and 7, showing quite stable modes.

7.4. Natural frequencies of a laminated plate

A [0/90/90/0] composite laminated simply supported plate is considered. The plate is a square with side a and thickness h. The side-to-thickness ratio a/h is taken as 10 to study the convergence

Table 4
[0°/90°/90°/0°] square laminated plate under sinusoidal load

$\frac{a}{h}$	Method	$\overline{w}$	$\overline{\sigma}_{xx}$	$\overline{\sigma}_{yy}$	$\overline{\tau}_{zx}$	$\overline{\tau}_{xy}$
4	3 strip [54]	1.8939	0.6806	0.6463	0.2109	0.0450
	HSDT [56]	1.8937	0.6651	0.6322	0.2064	0.0440
	FSDT [55]	1.7100	0.4059	0.5765	0.1398	0.0308
	Elasticity [57]	1.954	0.720	0.666	0.270	0.0467
	Ferreira et al. [37] ($N = 21$)	1.8864	0.6659	0.6313	0.1352	0.0433
	Ferreira (layerwise) [38] ($N = 21$)	1.9075	0.6432	0.6228	0.2166	0.0441
	Present (N=9)	1.9083	0.6433	0.6271	0.2172	0.0442
	Present ($N = 11$)	1.9091	0.6427	0.6262	0.2173	0.0443
	Present ($N = 15$)	1.9091	0.6429	0.6264	0.2173	0.0443
	Present ($N = 21$)	1.9091	0.6429	0.6265	0.2173	0.0443
10	3 strip [54]	0.7149	0.5589	0.3974	0.2697	0.0273
	HSDT [56]	0.7147	0.5456	0.3888	0.2640	0.0268
	FSDT [55]	0.6628	0.4989	0.3615	0.1667	0.0241
	elasticity [57]	0.743	0.559	0.403	0.301	0.0276
	Ferreira et al. [37] ($N = 21$)	0.7153	0.5466	0.4383	0.3347	0.0267
	Ferreira (layerwise) [38] ($N = 21$)	0.7309	0.5496	0.3956	0.2888	0.0273
	Present (N=9)	0.7297	0.5487	0.3965	0.2991	0.0273
	Present ($N = 11$)	0.7303	0.5486	0.3966	0.2994	0.0273
	Present ($N = 15$)	0.7303	0.5487	0.3966	0.2993	0.0273
	Present ($N = 21$)	0.7303	0.5487	0.3966	0.2993	0.0273
20	3 strip [54]	0.5061	0.5523	0.3110	0.2883	0.0233
	HSDT [56]	0.5060	0.5393	0.3043	0.2825	0.0228
	FSDT [55]	0.4912	0.5273	0.2957	0.1749	0.0221
	Elasticity [57]	0.517	0.543	0.309	0.328	0.0230
	Ferreira (layerwise) [38] ($N = 21$)	0.5121	0.5417	0.3056	0.3248	0.0230
	Ferreira et al. [37] ($N = 21$)	0.5070	0.5405	0.3648	0.3818	0.0228
	Present (N=9)	0.5104	0.5400	0.3061	0.3247	0.0228
	Present ($N = 11$)	0.5112	0.5407	0.3075	0.3257	0.0230
	Present ($N = 15$)	0.5113	0.5407	0.3073	0.3256	0.0230
	Present ($N = 21$)	0.5113	0.5407	0.3073	0.3256	0.0230
100	3strip [54]	0.4343	0.5507	0.2769	0.2948	0.0217
	HSDT [56]	0.4343	0.5387	0.2708	0.2897	0.0213
	FSDT [55]	0.4337	0.5382	0.2705	0.1780	0.0213
	Elasticity [57]	0.4347	0.539	0.271	0.339	0.0214
	Ferreira et al. [37] ($N = 21$)	0.4365	0.5413	0.3359	0.4106	0.0215
	Ferreira (layerwise) [38] ($N = 21$)	0.4374	0.5420	0.2697	0.3232	0.0216
	Present (N=9)	0.4350	0.5324	0.2689	0.3401	0.0207
	Present ($N = 11$)	0.4334	0.5385	0.2690	0.3335	0.0213
	Present ($N = 15$)	0.4347	0.5390	0.2709	0.3356	0.0214
	Present ($N = 21$)	0.4348	0.5391	0.2711	0.3359	0.0214

Table 5
Natural frequencies of a CCCC square Mindlin/Reissner plate with $h/a = 0.1, \nu = 0.3$

Mode no.	m	n	9×9	13×13	17×17	Rayleygh-Ritz [58]	Liew et al. [59]
1	1	1	1.6047	1.5937	1.5940	1.5940	1.5582
2	2	1	3.0417	3.0638	3.0653	3.0390	3.0182
3	1	2	3.0420	3.0641	3.0655	3.0390	3.0182
4	2	2	4.2224	4.3244	4.3245	4.2650	4.1711
5	3	1	4.9699	5.1054	5.1045	5.0350	5.1218
6	1	3	5.0382	5.1440	5.1448	5.0780	5.1594
7	3	2	5.9440	6.2066	6.1969		6.0178
8	2	3	5.9449	6.2074	6.1977		6.0178

Table 6
Natural frequencies of a CCCC square Mindlin/Reissner plate with $h/a = 0.01, \nu = 0.3$

Mode no.	m	n	9×9	13×13	17×17	21×21	Rayleygh-Ritz [58]	Liew et al. [59]
1	1	1	0.1005	0.1848	0.1753	0.1754	0.1754	0.1743
2	2	1	0.2761	0.3791	0.3576	0.3572	0.3576	0.3576
3	1	2	0.2761	0.3791	0.3576	0.3575	0.3576	0.3576
4	2	2	0.4827	0.5610	0.5283	0.5274	0.5274	0.5240
5	3	1	1.1254	0.6533	0.6435	0.6406	0.6402	0.6465
6	1	3	1.1344	0.6598	0.6464	0.6437	0.6432	0.6505
7	3	2	1.6041	0.7705	0.8145	0.8085		0.8015
8	2	3	1.6041	0.7705	0.8145	0.8099		0.8015

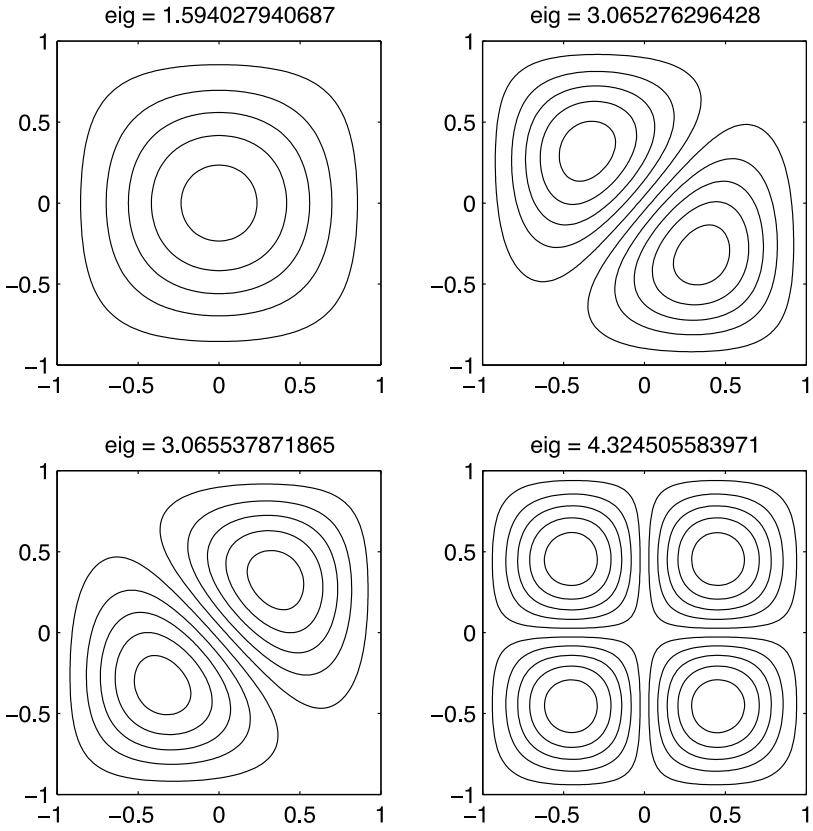

Fig. 2. Modes (1–4) of vibration of a CCCC square Mindlin/Reissner plate with $h/a = 0.1, \nu = 0.3$.

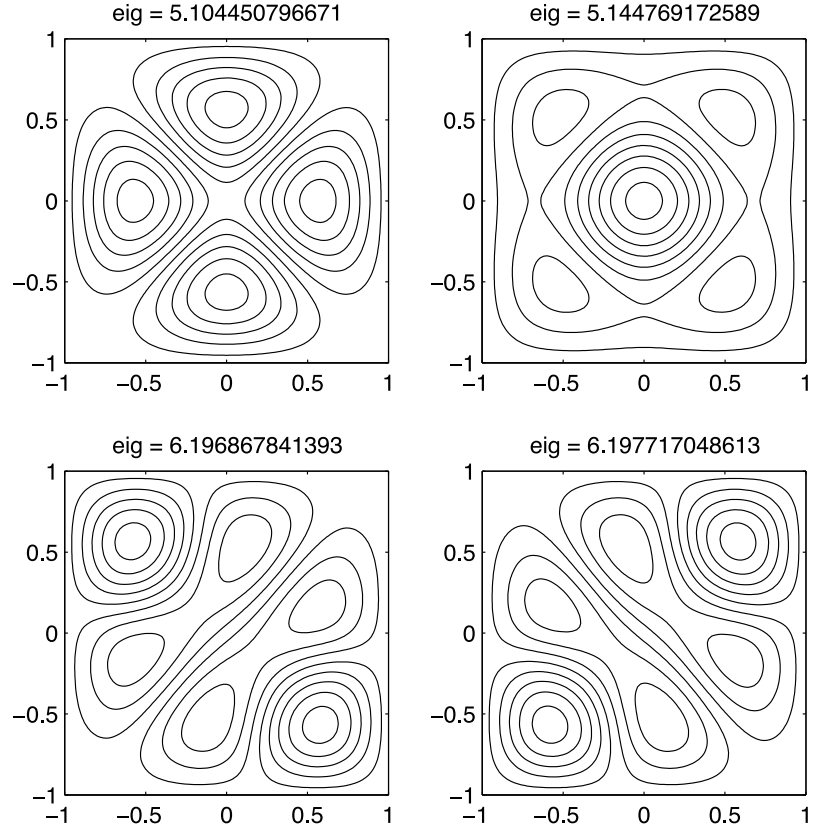

Fig. 3. Modes (5–8) of vibration of a CCCC square Mindlin/Reissner plate with $h/a = 0.1, \nu = 0.3$.

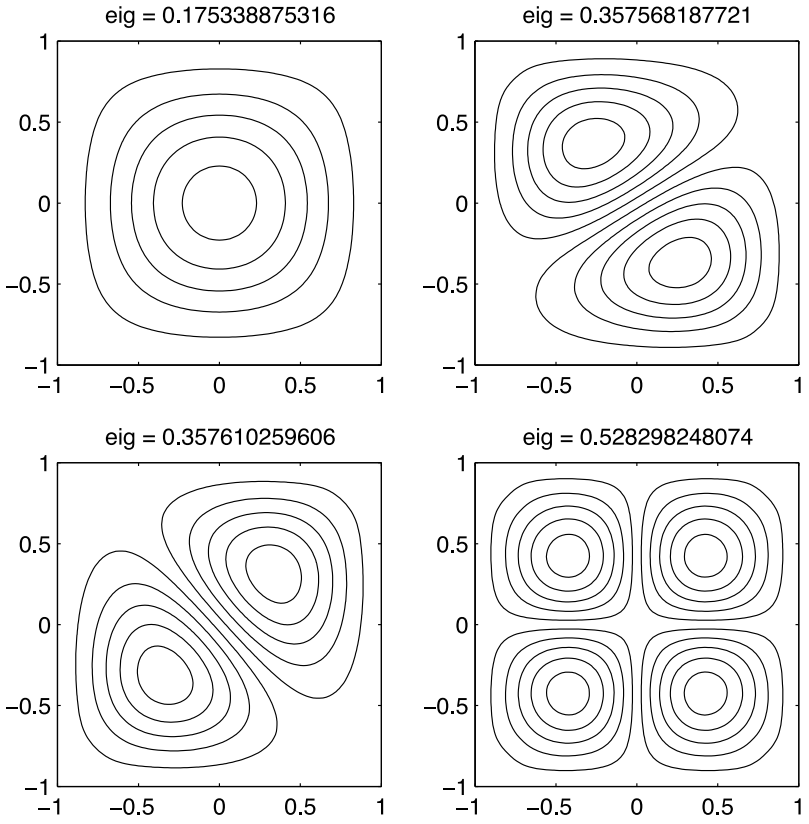

Fig. 4. Modes (1–4) of vibration of a CCCC square Mindlin/Reissner plate with $h/a = 0.01, \nu = 0.3$.

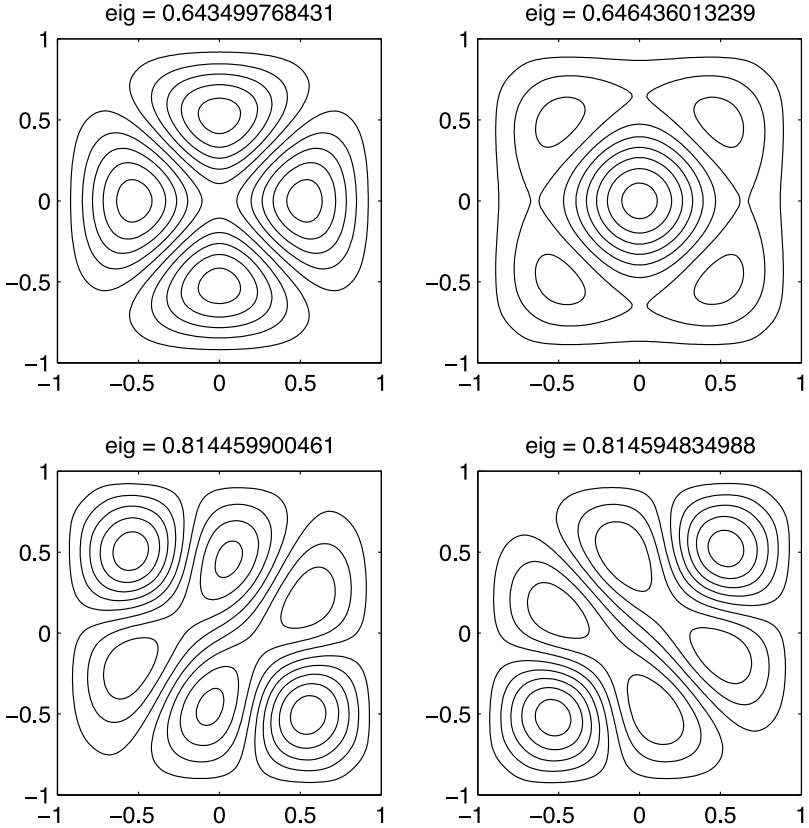

Fig. 5. Modes (5–8) of vibration of a CCCC square Mindlin/Reissner plate with $h/a = 0.01, \nu = 0.3$.

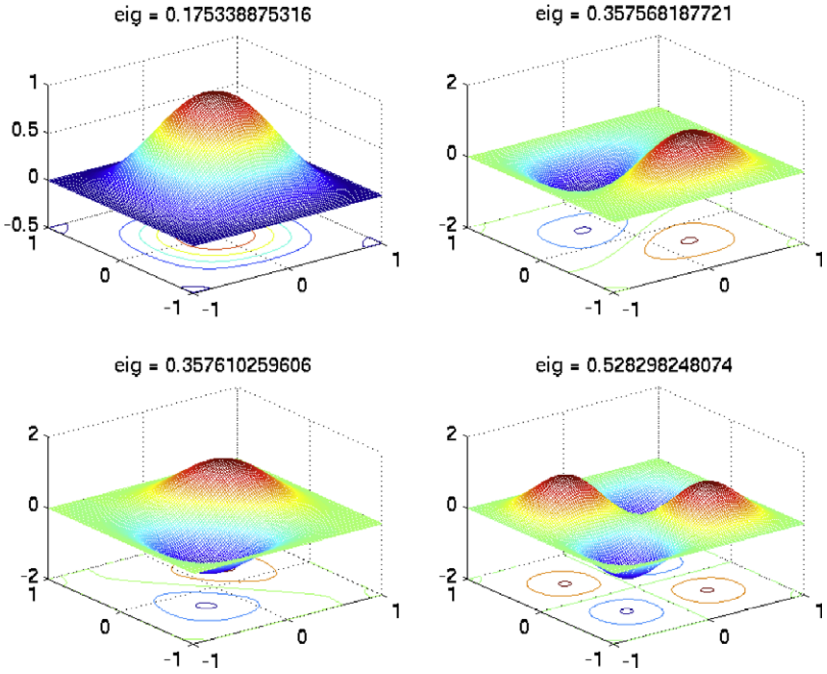

Fig. 6. Modes (1–4) of vibration of a CCCC square Mindlin/Reissner plate with $h/a = 0.01, \nu = 0.3$, 3D view.

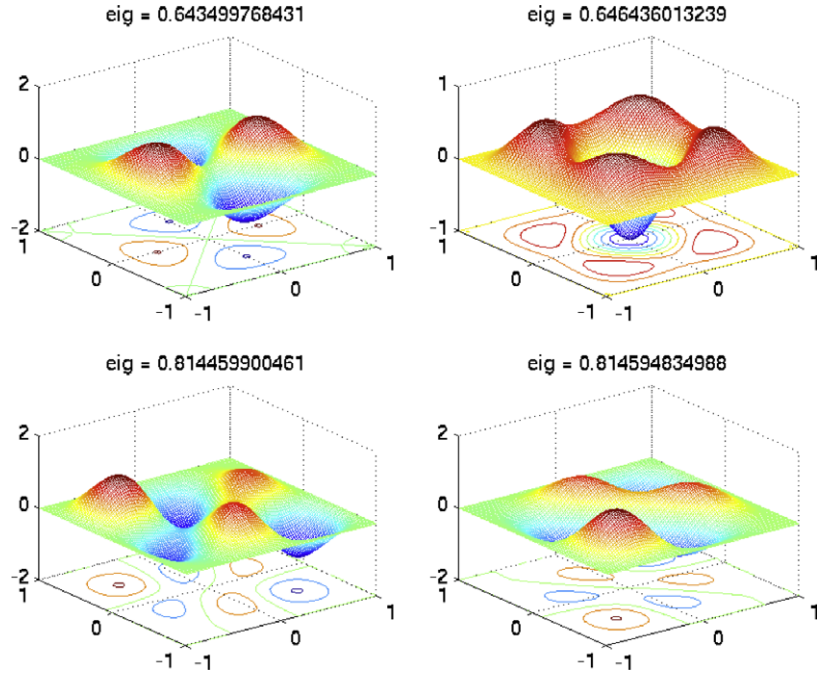

Fig. 7. Modes (5–8) of vibration of a CCCC square Mindlin/Reissner plate with $h/a = 0.01, \nu = 0.3$, 3D view.

Table 7
Convergence of the present layerwise method with respect to the number of nodes for a cross-ply laminate plate $(a/h = 10)$, $\bar{\omega} = \omega h\sqrt{\frac{\rho}{E_2}}$

Method/Mode	(1,1)	(1,2)	(2,1)	(2,2)	(1,3)	(2,3)	(3,1)	(3,2)
Exact (Srinivas et al. [60])	0.06715	0.12811	0.17217	0.20798				
HSDT (Nosier et al. [61])	0.06716	0.12816	0.17225	0.20808				
Layerwise (Wang and Zhang [62])	0.06716	0.12819	0.17230	0.20811	0.2287	0.2842	0.2936	0.3181
Present, layerwise (9×9)	0.0681	0.1321	0.1761	0.2154	0.2364	0.2960	0.2995	0.3290
Present, layerwise (11×11)	0.0681	0.1322	0.1762	0.2151	0.2377	0.2958	0.3010	0.3292
Present, layerwise (13×13)	0.0681	0.1322	0.1762	0.2150	0.2376	0.2954	0.3009	0.3288

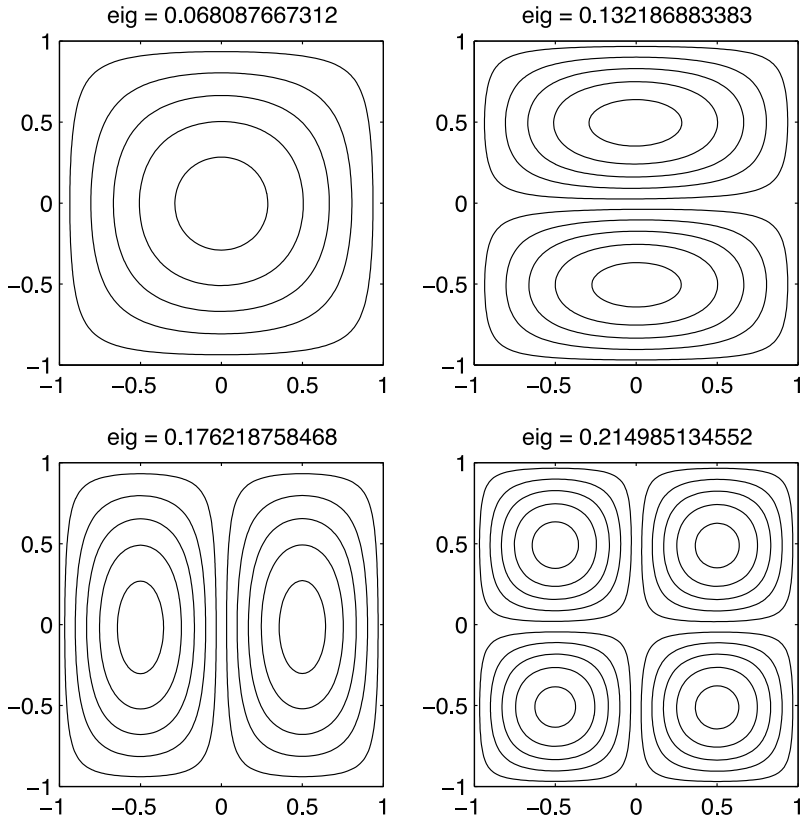

Fig. 8. First four modes of vibration: 2D view.

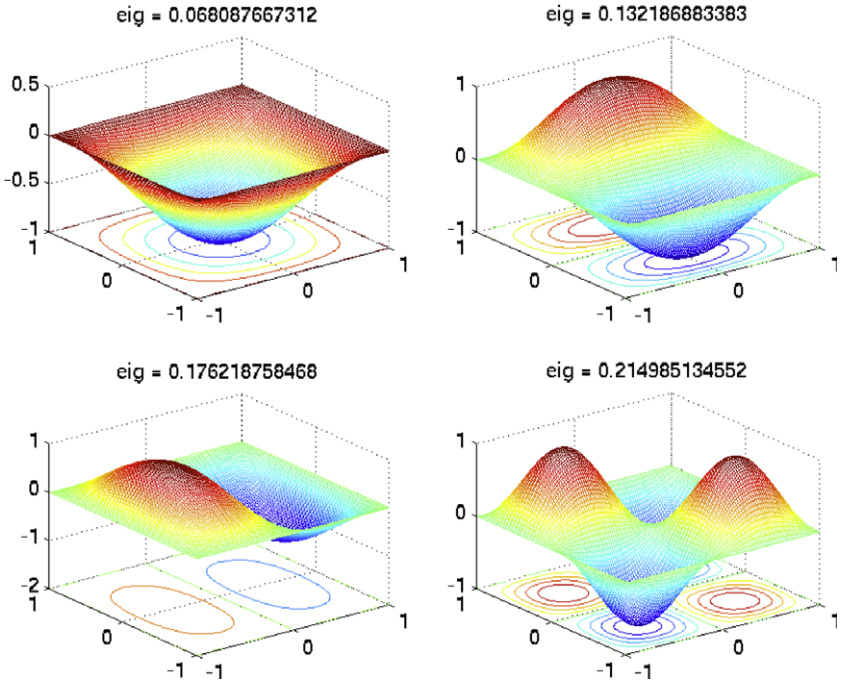

Fig. 9. First four modes of vibration.

with respect to the number of nodes. The thickness of each ply is $h/3$ and the material properties (MPa) are

$$E_1 = 173; \quad E_2 = 33.1; \quad G_{12} = 9.38; \quad G_{13} = 8.27; \quad G_{23} = 3.24;$$
$$\nu_{12} = 0.036; \quad \nu_{13} = 0.25; \quad \nu_{23} = 0.171. \tag{62}$$

The dimensionless frequency parameter is defined as

$$\bar{\omega} = \omega h \sqrt{\frac{\rho}{E_2}},$$

where ω is the circular frequency. Results from the present formulation are compared in Table 7 with those from the exact solution

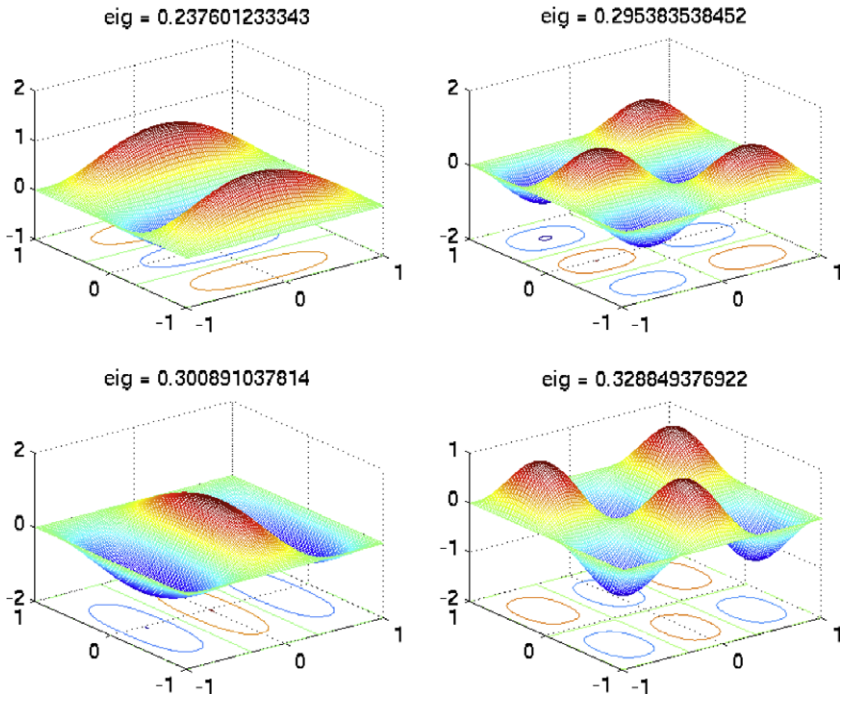

Fig. 10. Modes (5–8) of vibration.

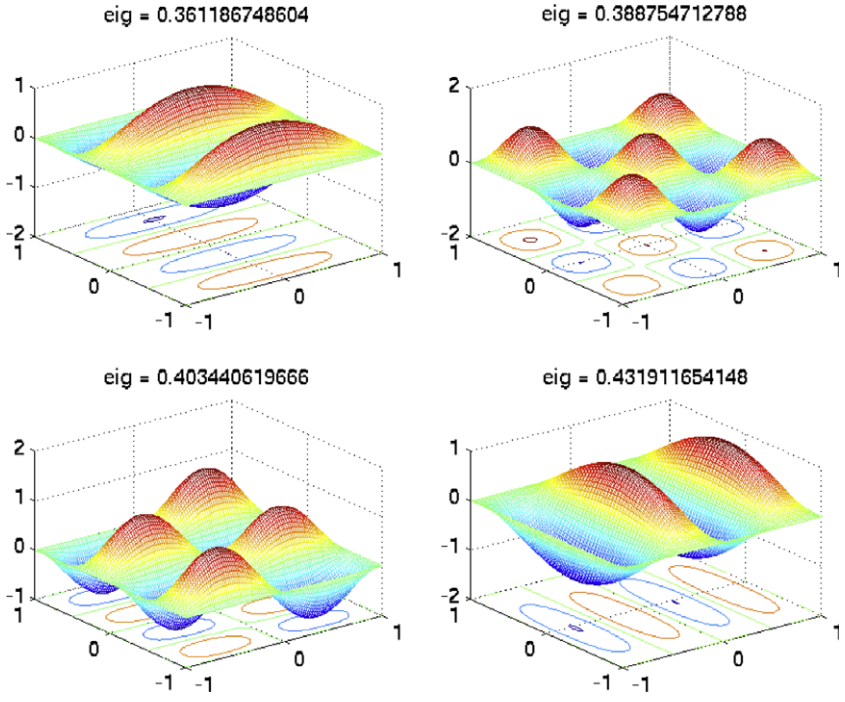

Fig. 11. Modes (9–12) of vibration.

by Srinivas et al. [60], a higher-order formulation by Nosier et al. [61] and a layerwise B-spline finite strip method by Wang and Zhang [62]. The present layerwise method produces convergent and highly accurate results for cross-ply laminated plates. All modes are accurately represented. Results from the present layerwise approach agree very well those from with the layerwise approach of Wang and Zhang [62].

In Fig. 8, the first four modes of vibration are illustrated for the 13×13 grid. The regular evolution of modes is noticeable. In Figs. 9–11, the first 12 modes in 3D view and their projections on the horizontal plane are illustrated.

We note that radial basis functions coupled with weak formulation of the governing equations of a higher-order shear and normal deformable plate theory have been employed in [64,65] to study deformations of a plate. Also, frequencies of a plate derived by using basis functions obtained by the moving least squares (MLS) approximation have been found to match well with those from the analytical solution of the problem [66,67]. It will be interesting

to investigate if the present RBFs-PS formulation will give as accurate values of the stress intensity factor as those obtained in [68] by using the MLS basis functions.

8. Conclusions

The first-order and the third-order shear deformation theories are laminate-wise, with laminate degrees of freedom, where all layers have the same rotations. Layerwise formulations can accommodate better the deformation behaviour of some laminates, particularly the sandwich laminates, where the core and the skin materials are very different.

In this paper, the free vibration analysis of composite laminated plates by the use of RBFs in a pseudospectral framework [63,19] and using a layerwise theory with independent rotations in each layer is performed for the first time.

The equations of motion were derived and solved by the collocation method. Boundary conditions interpolation was schematically formulated.

Composite laminated plates and sandwich plates were considered for testing the present methodology, and results obtained showed excellent accuracy for all cases. The method produces highly accurate results for isotropic, laminated composites and sandwich plates. The shape parameter of the basis functions is automatically selected by cross-validation techniques.

Acknowledgements

RCB's work was partially supported by the ONR grant N00014-98-06-0567 to Virginia Polytechnic Institute and State University.

References

[1] Whitney JM. The effect of transverse shear deformation in the bending of laminated plates. J Compos Mater 1969;3:534–47.
[2] Reissner E. A consistent treatment of transverse shear deformations in laminated anisotropic plates. AIAA J 1972;10(5):716–8.
[3] Reddy JN. Energy and variational methods in applied mechanics. New York: John Wiley; 1984.
[4] Sun CT. Theory of laminated plates. J Appl Mech 1971;38:231–8.
[5] Whitney JM, Sun CT. A higher order theory for extensional motion of laminated anisotropic shells and plates. J Sound Vib 1973;30:85–97.
[6] Mau ST. A refined laminate plate theory. J Appl Mech 1973;40:606–7.
[7] Christensen RM, Lo KH, Wu EM. A high-order theory of plate deformation, part 1: homogeneous plates. J Appl Mech 1977;44(7):663–8.
[8] Christensen RM, Lo KH, Wu EM. A high-order theory of plate deformation, part 2: laminated plates. J Appl Mech 1977;44(4):669–76.
[9] Reddy JN. A simple higher-order theory for laminated composite plates. J Appl Mech 1984;51:745–52.
[10] Reddy JN. A refined nonlinear theory of plates with transverse shear deformation. Int J Solids Struct 1984;20(9/10):881–906.
[11] Reddy JN. Mechanics of laminated composite plates. New York: CRC Press; 1997.
[12] Chou PC, Corleone J. Transverse shear in laminated plate theories. AIAA J 1973:1333–6.
[13] Di Sciuva M. An improved shear-deformation theory for moderately thick multilayered shells and plates. J Appl Mech 1987;54:589–97.
[14] Murakami H. Laminated composite plate theory with improved in-plane responses. J Appl Mech 1986;53:661–6.
[15] Ren JG. A new theory of laminated plate. Compos Sci Technol 1986;26:225–39.
[16] Carrera E. Historical review of zig-zag theories for multilayered plates and shells. Appl Mech Rev 2003(56):287–308.
[17] Hardy RL. Multiquadric equations of topography and other irregular surfaces. Geophys Res 1971;176:1905–15.
[18] Hardy RL. Theory and applications of the multiquadric-biharmonic method: 20 years of discovery. Comput Math Appl 1990;19(8/9):163–208.
[19] Kansa EJ. Multiquadrics – a scattered data approximation scheme with applications to computational fluid dynamics. I: surface approximations and partial derivative estimates. Comput Math Appl 1990;19(8/9): 127–45.
[20] Kansa EJ. Multiquadrics – a scattered data approximation scheme with applications to computational fluid dynamics. II: solutions to parabolic, hyperbolic and elliptic partial differential equations. Comput Math Appl 1990;19(8/9):147–61.
[21] Liu GR. Mesh free methods. Boca Raton, USA: CRC Press; 2003.
[22] Liu GR, Dai KY, Lim KM, Gu YT. A radial point interpolation method for simulation of two-dimensional piezoelectric structures. Smart Mater Struct 2003;12:171–80.
[23] Gu YT, Liu GR. A boundary radial point interpolation method (brpim) for 2-D structural analyses. Struct Eng Mech 2003;15(5):535–50.
[24] Liu GR, Yan L, Wang JG. Point interpolation method based on local residual formulation using radial basis functions. Struct Eng Mech 2003;14(6):713–32.
[25] Wu YL, Liu GR. A meshfree formulation of local radial point interpolation method (lrpim) for incompressible flow simulation. Comput Mech 2003;30(5-6):355–65.
[26] Liu GR, Gu YT. A meshfree method: meshfree weak–strong (mws) form method, for 2-D solids. Comput Mech 2003;33(1):2–14.
[27] Liu GR, Dai KY, Lim KM, Gu YT. Comparison between the radial point interpolation and the kriging interpolation used in meshfree methods. Comput Mech 2003;32(1-2):60–70.
[28] Hon YC, Lu MW, Xue WM, Zhu YM. Multiquadric method for the numerical solution of byphasic mixture model. Appl Math Comput 1997;88:153–75.
[29] Hon YC, Cheung KF, Mao XZ, Kansa EJ. A multiquadric solution for the shallow water equation. ASCE J Hydraul Eng 1999;125(5):524–33.
[30] Wang JG, Liu GR, Lin P. Numerical analysis of biot's consolidation process by radial point interpolation method. Int J Solids Struct 2002;39(6):1557–73.
[31] Ferreira AJM, Martins PALS, Roque CMC. Solving time-dependent engineering problems with multiquadrics. J Sound Vib 2005;280:595–610.
[32] Liu GR, Gu YT. A local radial point interpolation method (lrpim) for free vibration analyses of 2-D solids. J Sound Vib 2001;246(1):29–46.
[33] Liu GR, Wang JG. A point interpolation meshless method based on radial basis functions. Int J Numer Meth Eng 2002;54:1623–48.
[34] Wang JG, Liu GR. On the optimal shape parameters of radial basis functions used for 2-D meshless methods. Comput Meth Appl Mech Eng 2002;191:2611–30.
[35] Ferreira AJM. A formulation of the multiquadric radial basis function method for the analysis of laminated composite plates. Compos Struct 2003;59:385–92.
[36] Ferreira AJM. Thick composite beam analysis using a global meshless approximation based on radial basis functions. Mech Adv Mater Struct 2003;10:271–84.
[37] Ferreira AJM. Roque CMC, Martins PALS. Analysis of composite plates using higher-order shear deformation theory and a finite point formulation based on the multiquadric radial basis function method. Compos: Part B 2003;34:627–36.
[38] Ferreira AJM. Analyis of composite plates using a layerwise deformation theory and multiquadrics discretization. Mech Adv Mater Struct 2005;12(2):99–112.
[39] Ferreira AJM. Polyharmic (thin-plate) splines in the analysis of composite plates. Int J Mech Sci 2004;46(10):1549–69.
[40] Fornberg B. A practical guide to pseudospectral methods. Cambridge University Press; 1998.
[41] Trefethen LN. Spectral methods in matlab. Philadelphia, PA: SIAM; 2000.
[42] Fasshauer GE. Meshfree approximation methods with matlab, interdisciplinary mathematical sciences, vol. 6. Singapore: World Scientific Publishers; 2007.
[43] Driscoll TA, Fornberg B. Interpolation in the limit of increasingly flat radial basis functions. Comput Math Appl 2002;43:413–22.
[44] Larsson E, Fornberg B. Theoretical and computational aspects of multivariate interpolation with increasingly flat radial basis functions. Comput Math Appl 2005;49:103–30.
[45] Schaback R. Multivariate interpolation by polynomials and radial basis functions. Constr Approx 2005;21:293–317.
[46] Fasshauer GE. Collocation methods as pseudospectral methods. In: Kassab A, Brebbia CA, Divo E, Poljak D, editors. Boundary elements. Southampton: WIT Press; 2005. p. 47–56.
[47] Fasshauer GE. RBF collocation methods and pseudospectral methods. preprint, 2004.
[48] Platte RB, Driscoll TA. Eigenvalue stability of radial basis function discretizations for time-dependent problems. Comput Math Appl 2006;51(8):1251–68.
[49] Schaback R. On the efficiency of interpolation by radial basis functions. In: Le MThautT A, Rabut C, Schumaker LL, editors. Proceedings of surface fitting and multiresolution methods. Vanderbilt University Press; 1997. p. 309–18.
[50] Rippa S. An algorithm for selecting a good value for the parameter *c* in radial basis function interpolation. Adv Comput Math 1999;11:193–210.
[51] Srinivas S. A refined analysis of composite laminates. J Sound Vib 1973;30:495–507.
[52] Pandya BN, Kant T. Higher-order shear deformable theories for flexure of sandwich plates-finite element evaluations. Int J Solids Struct 1988;24:419–51.
[53] Ferreira AJM, Barbosa JT. Buckling behaviour of composite shells. Compos Struct 2000;50:93–8.
[54] Akhras G, Cheung MS, Li W. Finite strip analysis for anisotropic laminated composite plates using higher-order deformation theory. Comput Struct 1994;52(3):471–7.
[55] Akhras G, Cheung MS, Li W. Static and vibrations analysis of anisotropic laminated plates by finite strip method. Int J Solids Struct 1993;30(22):3129–37.
[56] Reddy JN. A simple higher-order theory for laminated composite plates. J Appl Mech 1984;51:745–52.

[57] Pagano NJ. Exact solutions for rectangular bidirectional composites and sandwich plates. J Compos Mater 1970;4:20–34.
[58] Dawe DJ, Roufaeil OL. Rayleigh–Ritz vibration analysis of mindlin plates. J Sound Vib 1980;69(3):345–59.
[59] Liew KM, Wang J, Ng TY, Tan MJ. Free vibration and buckling analyses of shear-deformable plates based on fsdt meshfree method. J Sound Vib 2004;276:997–1017.
[60] Srinivas S, Rao CVJ, Rao AK. An exact analysis for vibration of simply-supported homogeneous and laminated thick rectangular plates. J Sound Vib 1970;12(2):187–99.
[61] Nosier A, kapania RK, Reddy JN. Free vibration analysis of laminated plates using a layerwise theory. AIAA J 1993;31(2):2335–46.
[62] Wang S, Zhang Y. Vibration analysis of rectangular composite laminated plates using layerwise B-spline finite strip method. Compos Struct 2005;68(3):349–58.
[63] Fasshauer GE. Solving partial differential equations by collocation with radial basis functions. Surface fitting and multiresolution methods. In: Proceedings of the 3rd international conference on curves and surfaces, vol. 2; 1997. p. 131–8.
[64] Xiao JR, Gilhooley DF, Batra RC, Gillespie Jr JW, McCarthy MA. Analysis of thick composite laminates using a higher-order shear and normal deformable plate theory (HOSNDPT) and a meshless method. Compos: Part B 2008;39:414–27.
[65] Gilhooley DF, Batra RC, Xiao JR, McCarthy MA, Gillespie Jr JW. Analysis of thick functionally graded plates by using higher-order shear and normal deformable plate theory and MLPG method with radial basis functions. Compos Struct 2007;80:539–52.
[66] Qian LF, Batra RC, Chen LM. Free and forced vibrations of thick rectangular plates by using higher-order shear and normal deformable plate theory and meshless petrov-galerkin (MLPG) method. CMES 2003;4:519–34.
[67] Qian LF, Batra RC. Design of bidirectional functionally graded plate for optimal natural frequencies. J Sound Vib 2005;280:415–24.
[68] Batra RC, Ching HK. Analysis of elastodynamic deformations near a crack/notch tip by the meshless local petrov-galerkin (MLPG) method. CMES 2002;3:717–30.